4. The stability analyses imply that an arcade can become unstable when either its height or twist or plasma pressure become too great.

1.3 PREFLARE MAGNETIC AND VELOCITY FIELDS

M.J. Hagyard, V. Gaizauskas, G.A. Chapman, A.C. deLoach, G.A. Gary, H.P. Jones, J.T. Karpen, M.-J. Martres, J.G. Porter, B. Schmieder, J.B. Smith, Jr., and J. Toomre

A description of the structure, dynamics and energetics of the preflare state depends on our ability to characterize the magnetic and velocity fields of the preflare active region. In this SMM Workshop, we fortunately had at our disposal many sets of coordinated SMM and ground-based observations of magnetic and velocity fields from the photosphere, chromosphere, transition region and corona to aid in this characterization. At the outset we decided that several aspects of these fields are of special interest to the preflare state: configurations in the magnetic and velocity fields that seem peculiar to flaring active regions; the existence of shears (in both the magnetic and velocity fields); the occurrence of emerging flux. Some questions naturally arise concerning these topics. Do flares occur in active regions where the magnetic field is force-free (currents are field-aligned), non-force-free or both? If it is force-free, can it be specified by a constant-alpha? [Alpha is the ratio between current density and field strength]. Is magnetic shear correlated with the occurrence of flares and, if so, is there a critical value of this shear? What is the role of the resulting electric currents? What are the preflare characteristics of the velocity field and how do they evolve? What is the spatial and physical correlation between sheared velocity and magnetic fields? What are the conditions necessary for emerging flux to trigger a flare? What growth rates of flux are significant? How does the flux emerge into the corona?

Although we did not find answers to all these questions, we made significant progress in many areas. We found that the preflare active region is very dynamic, exhibiting recurrent mass surges and intermittent heating events at many sites. In one case, that of an active region not particularly productive of large flares, the structure of the magnetic field was best represented by a nonlinear force-free field; for a particularly flare-productive region, there were indications that, subject to certain restrictions on the boundary conditions, the field was non-force-free, exhibiting a measurable Lorentz force. We also found that both the magnetic and velocity fields are sheared in flaring regions; the shear of the magnetic field attained maximum values at the sites of flare onset, whereas the velocity field sometimes exhibited an unusual vortical structure at these sites. These sheared magnetic fields produced persistent, large-scale concentrations of electric currents at the flare sites; numerical values for the magnitudes of these currents provided input to models describing preflare brightenings based on joule heating or current-driven instabilities. Finally, we found the role of emerging flux in flares to be ambivalent, providing an obvious triggering of some classes of flare while having no role in the flare process in others.

In describing these various results the material has been arranged as follows. We begin with a characterization of the preflare magnetic field, using theoretical models of force-free fields together with observed field structure to determine the general morphology. We then present direct observational evidence for sheared magnetic fields. The role of this magnetic shear in the flare process is considered within the context of an MHD model that describes the buildup of magnetic energy, and the concept of a critical value of shear is explored. The related subject of electric currents in the preflare state is discussed next, with emphasis on new insights provided by direct calculations of the vertical electric current density from vector magnetograph data and on the role of these currents in producing preflare brightenings. Next we discuss results from our investigations concerning velocity fields in flaring active regions, describing observations and analyses of preflare ejecta, sheared velocities, and vortical motions near flaring sites. This is followed by a critical review of prevalent concepts concerning the association of flux emergence with flares.

1.3.1 General Morphology of the Preflare Magnetic Field

It is generally accepted that magnetic fields are the ultimate source of the energy released in a flare (e.g., Svestka, 1976) and that this energy is stored in an active region prior to the flare as a result of the stressing of these fields into non-potential configurations We have accumulated observational evidence for such stressed fields, both on large and small scales, and studied the stressing processes which result in the eruption of a flare. We first discuss our studies of the general morphology of the preflare magnetic field.

A. Gary endeavored to classify the non-potential character of magnetic fields in active regions assuming that the fields are force-free, i.e., that the following relation is valid:

$$\nabla \times \underset{\sim}{B} = \mu_0 \underset{\sim}{J} = \alpha \underset{\sim}{B}. \qquad (1.3.1)$$

Several active regions observed during SMM were modeled using the force-free formulation developed by Nakagawa and Raadu (1972), who assumed that the parameter α is spatially invariant. One of these regions, AR2684, was of particular interest since it was observed by instruments on a Lockheed rocket flight at 20:30 UT on September 23, 1980, as well as by SMM and ground-based instruments. Although the flare activity in the region was relatively minor, several C- and M-class flares occurred on the 23rd and 24th, the largest being a 1B/M1 event at 07:28 UT on the 24th.

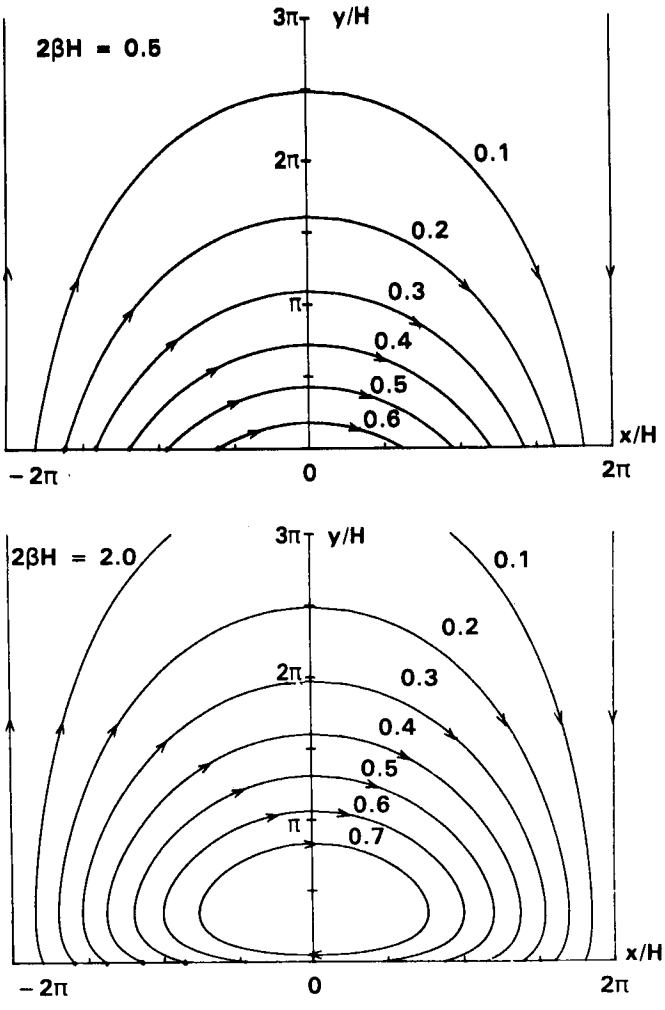

Figure 1.2.10 The magnetic field lines of the equilibria (1.2.5) have the form (a) when the base pressure is so small that $2\beta H < 1.15$, (b) when $1.15 < 2\beta H < \pi$. (From Hood, 1983b).

Raadu type with the magnetic field lines crossing through the prominence in the opposite direction. Leroy, Bommier, and Sahal-Brechot (1984) find observationally that those of Kuperus-Raadu type are, somewhat surprisingly, twice as common. Also, observations of slow steady upflows in prominences when seen on the disc can be explained by a dynamic prominence model in which the magnetic field evolves in response to photospheric motions. The large quiescent prominences are mainly of Kuperus-Raadu type and the footpoint motions would need to be convergent, which suggests that such prominences lie at the boundaries of large-scale giant cells. By comparison, the plage filaments have a Kippenhahn-Schluter field orientation and would need divergent footpoint motions. At present, Malherbe, Forbes and Priest are studying numerically the formation of prominences in current sheets by radiative tearing. They have adopted the previous radiative code of Forbes and Priest (1982, 1983a, 1983b) to include an energy equation with Joule heating, coronal heating and radiative cooling. In particular, the cases when the cooling time is a factor of between 0.1 and 10 times the tearing times are being investigated.

1.2.7 Conclusion

During the Workshop there have been major advances in the theory of magnetic reconnection and of magnetic instability, with important implications for the observations, as follows:

1. Fast and slow magnetic shock waves are produced by the magnetohydrodynamics of reconnection and are potential particle accelerators.
2. The impulsive bursty regime of reconnection gives a rapid release of magnetic energy in a series of bursts.
3. The radiative tearing mode creates cool filamentary structures in the reconnection process.

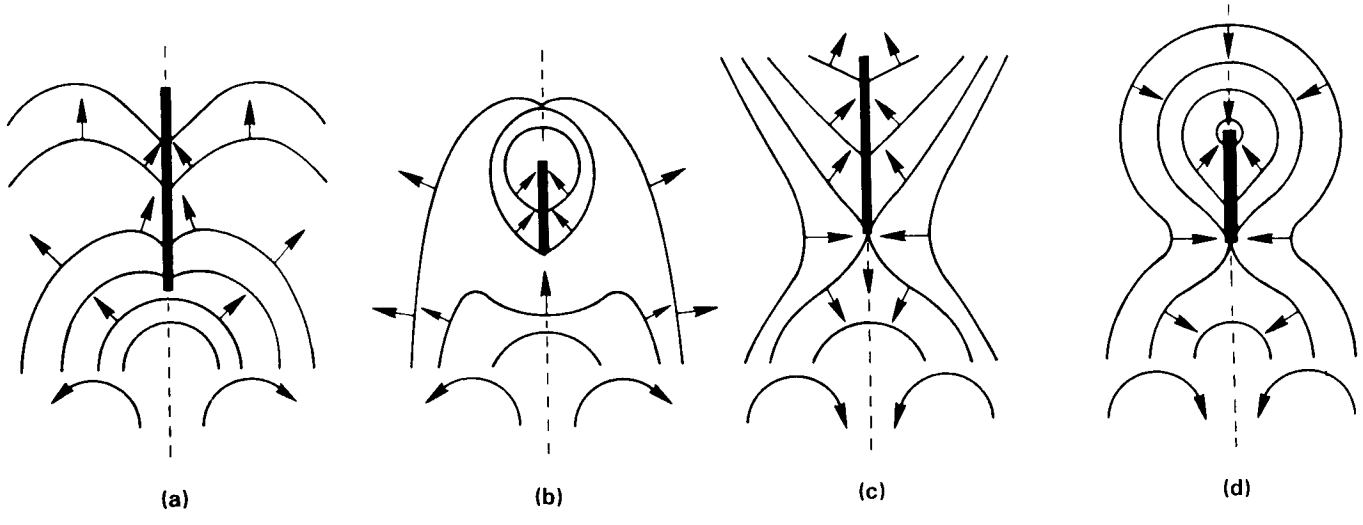

Figure 1.2.11 Current sheet models of prominences.

This coordinated observational program produced UVSP, XRP AND HXIS data from SMM, Lyman-alpha and 1600 Å spectroheliograms from the rocket experiments, and magnetic field, H-alpha and He 10830 Å data from the ground-based observatories; B. Haisch assembled these data for the workshop. It was hoped that chromospheric and coronal filamentary structure would delineate both footpoints and field lines of the magnetic field of the entire active region. Then, using these inferred structures, the most appropriate value of the parameter alpha could be selected, i.e., the one that matched calculated field lines with the observed ones. A similar method was used extensively in analyses of Skylab data to model the magnetic field of active regions. The basic observational data used in the analyses are shown in Figure 1.3.1a. The bright points observed in the 1600 Å spectroheliograms were assumed to be footpoints of the Lyman-alpha loops and H-alpha fibrils and were thus used as the initial coordinates of the field line calculations for various constant-alpha computations. As expected, Gary found that the field lines calculated for a single value of alpha would not fit all of the observed structures. In Figure 1.3.1b, areas are indicated where field lines calculated for different alphas showed good agreement with the observed fibrilar orientations. Although there are areas of positive, negative and zero alpha, a dominance of positive alpha is indicated. Because the "footpoints" used in the calculations were generally outside the sunspots, this "alpha map" applies only to the weaker field areas.

To investigate the non-potential character of the region's magnetic field without resorting to an assumption of constant alpha, Gary compared the direction (azimuth) of the observed transverse field in the photosphere with that of a potential field distribution. The use of the azimuth of the transverse field as an indicator of the non-potential character of the field is based on the observation that the projected field lines from the force-free calculations were parallel to the observed azimuthal directions; the only exceptions were the field lines that rose very high into the corona and whose lengths were characteristic of the scale of the magnetogram's field-of-view. In his analysis, Gary found the deviation of the observed azimuth from a potential orientation at each grid point, and assigned to these points a positive or negative sign depending on the sense of the observed deviation or "twist"; the results are shown in Figure 1.3.1c. Since this "alpha map" only pertains to the regions in and near the sunspots where the transverse field is above 200 G, it is difficult to relate it to the alpha map in Figure 1.3.1b for the areas of the weaker fields. However, where there is some overlap, the two methods give consistent results, and confirm that a constant alpha force-free field cannot characterize the magnetic topology of this active region.

A second region of interest, AR 2372 (very flare-productive on the solar disk in early April 1980), also proved difficult to model, but for another reason. As will be discussed in Section 1.3.2.2, this region exhibited a large degree of shear in its magnetic field in the area of a magnetic δ-configuration (umbrae of opposite polarity within the same penumbra). This extreme shear could not be reproduced with the linear force-free computation of Nakagawa and Raadu because of the limitations on the maximum value of alpha (i.e., twist or shear). In their formulation, alpha must be less than $2\pi/L$, where L is the scale of the magnetogram. However, an analysis by Krall (private communication) produced some evidence that the magnetic field in the area of the δ-configuration was non-force-free. Using transverse field measurements obtained with the MSFC vector magnetograph, he calculated the resultant Lorentz force in the region of the delta from a formulation derived by Molodensky (1974). Krall found this force had a non-zero horizontal component that was consistent with the observed sunspot motions in that area.

These attempts to model the magnetic fields indicate that, for a moderately active region, the structure of its field was fairly well represented by a nonlinear force-free field. On the other hand, calculations based on the observed field of a highly flare-productive region resulted in a non-zero Lorentz force. Until analyses of other regions are available, these results must be regarded as very preliminary.

1.3.2 Magnetic Field Shear

1.3.2.1 Evidence for Sheared Magnetic Fields

Storage of flare energy in stressed magnetic fields arises from the increasing deformation of the magnetic field from a potential configuration. This deformation can occur, for instance, through the shearing of magnetic loops as a result of footpoint translations, or through the twisting of individual loops rooted in sunspots which rotate. Some of our indirect evidence for preflare energy storage in stressed fields comes from the geometry of fibrils and structures within filaments in the vicinity of flares; these fibrils and filamentary structures presumably delineate the chromospheric magnetic field. For example, in a detailed study of the August 1972 flares, Zirin and Tanaka (1973) inferred the presence of strongly-sheared, transverse magnetic fields from the twisted appearance of penumbral filaments. In more recent work using both SMM and ground-based observations, Athay *et al.* (1984) determined the broad features of the magnetic field geometry from chromospheric and transition region Dopplergrams, assuming that the fluid flow follows magnetic lines of force. H-alpha filament orientation and motion, and the relationship of the filaments to sunspots provided additional information on the field geometry. From these data, they deduced that pronounced magnetic shear was present at transition region heights over the entire length of a prominent segment of the polarity-inversion line. This shear remained relatively steady for periods of several days except for temporary local disruptions due to emerging flux regions (see Section 1.3.4.2).

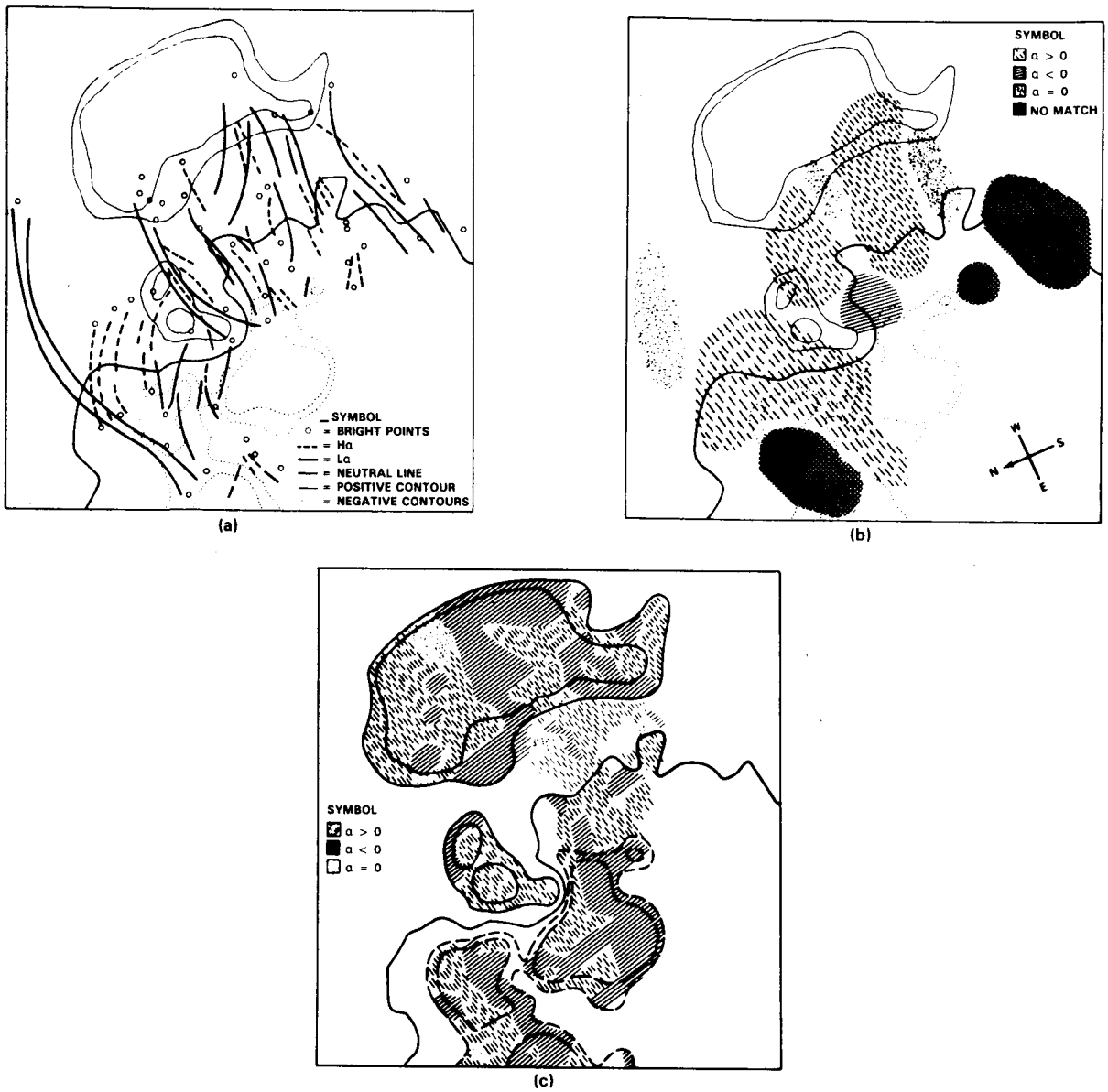

Figure 1.3.1 Force-free field modeling of AR 2684 for September 23, 1980. (a) The filamentary structures inferred from H- α and Lyman- α spectroheliograms are shown superposed on a plot of the photospheric line-of-sight magnetic field of the region, which was located at N18W22. Also shown are the bright points observed in the 1600 A spectroheliograms. The solid (dashed) magnetic field contours represent positive (negative) field levels of 250 and 500 G; the solid curve separating positive and negative fields is the magnetic neutral line. The field-of-view is 2.5′ × 2.5′ and the solar orientation is as shown in panel b. (b) Regions are specified where the fibrilar structures of panel a are matched (or not matched) by force-free field lines calculated with positive, negative or zero (potential field) values of the parameter alpha. The symbols are shown in the upper right corner of the panel; cross-hatched areas specify regions where the fibrils and field lines could not be matched to within 45 degrees. The contours shown are identical to those in panel a. (c) Map of the differences between the orientations of the observed transverse field and a potential field, where the potential field fits the boundary conditions imposed by the observed line-of-sight field. Areas of positive, negative and zero deviations or "twist" are shown according to the legend for the parameter alpha since the force-free parameter alpha is also a measure of the twist of the field. Only areas for which the line-of-sight field is greater than 250 G are indicated, except for one region in which the transverse field was above 200 G. The contours shown are again those designated in panel a.

Based on such indirect indications of sheared magnetic fields, much of the previous modeling of preflare magnetic fields during the Skylab series of flare workshops was performed with the assumption that configurations of sheared magnetic fields did indeed exist in preflare active regions. Now, however, direct evidence for sheared magnetic loops comes from measurements of transverse magnetic fields in the photosphere near the magnetic neutral line. At the neutral line, the direction of the transverse component of the field will indicate the orientation of low-lying field loops which connect footpoints on opposite polarity sides. Initial observations of transverse field directions which appeared sheared relative to the neutral line were reported by Smith *et al.* (1979) using data from the NASA/Marshall Space Flight Center (MSFC) vector magnetograph (Hagyard *et al.*, 1983), which observes in the FeI 5250 A line originating in the photosphere. During SMM, many subsequent examples of sheared magnetic fields in a number of active regions, most of which produced flare activity, were reported by the MSFC group (Krall *et al.*, 1982; Patty and Hagyard, 1984; Smith, 1984 [private communication]).

1.3.2.2 Correlation with Flare Activity

These direct measurements of magnetic shear provide compelling evidence for linking magnetic shear with the incidence of flares. For example, in a statistical study J.B. Smith, Jr. (private communication) found a distinct preference for high flare productivity and major flares in areas with significant magnetic shear. In evolving regions, an increase in shear clearly accompanies an increase in flare frequency and magnitude, while decreasing shear is commonly accompanied by a decrease in flare production. To evaluate the magnetic shear, Smith used the vector MSFC magnetograms which depict the transverse fields at the photosphere as line segments. Their length and orientation give the strength and direction of the transverse field at each point in the field-of-view. The "angle of shear" along the neutral line can be determined by comparing the directions of the line segments to the orientation of the neutral line. This interpretation of shear assumes that line segments of a potential field cross the neutral line orthogonally.

Smith qualitatively evaluated several regions for correlation between this "angle of shear" and flare production. In two cases, a pair of regions were simultaneously visible, one with measurable shear and the other with fields that appeared more potential. In both cases, the region with observable shear produced flares while the other was essentially quiet. Perhaps the most notable example occurred in April 1980 when AR 2370, a large region promising significant activity but producing little of note, rotated onto the visible disk a few days before the birth nearby of AR 2372 early on the 4th of April. Following rapid development of the main spots of AR 2372, pronounced photospheric shearing motions were observed between the 5th and 7th of April for the sunspots of opposite polarities inside this region. During this epoch of spot motions, the transverse field directions indicated the presence of strong shear along the neutral line in relatively strong magnetic fields; flares, some major, were frequent (Krall *et al.*, 1982). A decrease in the shear of AR 2372 after the 7th was followed by a sharp decrease in flare production. Several other regions were analyzed with similar results: those with strongly sheared fields were flare productive while those with essentially potential fields (or weakly sheared fields) had only minor activity.

Smith also studied the development and evolution of shear within AR 2776, during November 1980 during SMM. The evolution of its vector magnetic field over the period November 2-5 is shown in Figure 1.3.2. On November 2nd (Figure 1.3.2a), some magnetic complexity was evident in the presence of a Δ configuration, although the surrounding magnetic gradients were moderate, the fields only moderately strong, and the field alignments generally appeared to be potential. This situation held also on the 3rd and 4th (Figures 1.3.2b,c) but with some complexity added by the building of the positive fields to the north. Still, the observed shear was not extensive. However, the changes between the 4th and 5th were striking, particularly in the pronounced shear seen in the near alignment of the transverse field with the entire length of the neutral line in the area of the delta on the 5th (Figures 1.3.2d,e). In addition, field strengths and gradients increased markedly from the 4th to the 5th. Smith examined the X-ray flares that occurred during the period November 1-12. He found that energetic soft X-ray flares (class M1 or greater) were infrequent until the 5th, when both frequency and magnitude rapidly increased and several major flares followed. Again, the correspondence of increased shear with increased flare activity is borne out by this study.

Smith also analyzed the magnetic shear in other active regions: AR 2522 (June 1980), AR 2544 (June/July 1980) and AR 2725 (October 1980). In Figure 1.3.3, the line-of-sight (B_L) and transverse (B_T) components of the magnetic fields of these three regions are shown along with the calculated vertical electric current densities, J_z. Varying degrees of magnetic complexity were reflected in the level of flare activity for two of the three regions; the third region was somewhat of an anomaly. AR 2725 (columns c and d in Figure 1.3.3) was the most magnetically complex and also the most flare productive. Examination of the transverse magnetic field data revealed significant shear and moderate field strengths along that portion of the neutral line to the left of center in the magnetograms where the flare of October 11 at 17:41 UT (classified as 1B/C7) occurred, as determined from SMM soft X-ray data. Although significant flares were infrequent, a few class M X-ray flares were observed and a major flare (3B/X3) occurred on October 14. AR 2522 (column a in Figure 1.3.3) has the complexity of a convoluted neutral line and an isolated island of positive polarity, but

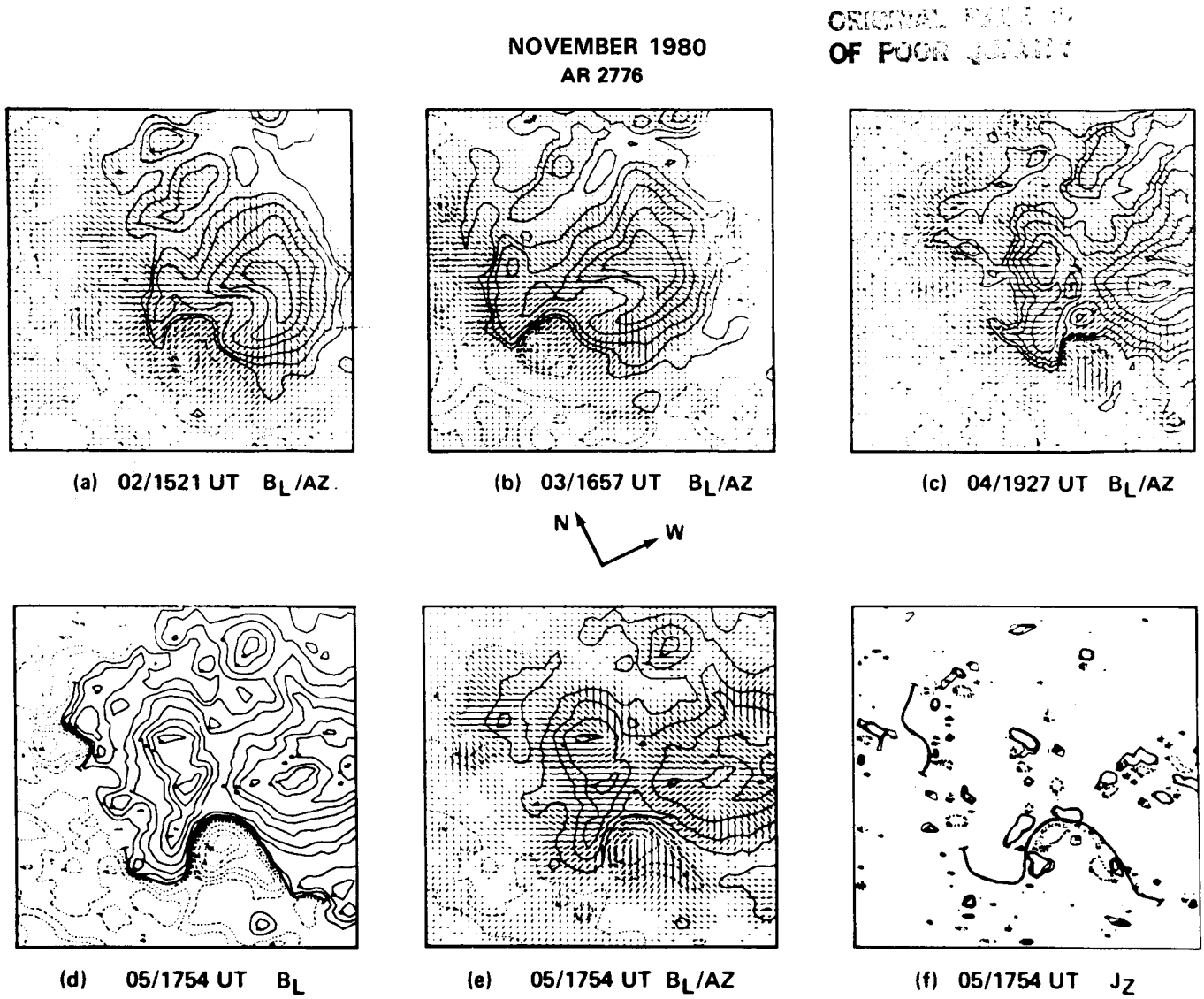

Figure 1.3.2 Magnetic evolution of AR 2776 over the period November 2-5, 1980. The field-of-view in all panels is approximately 2.1′ × 2.1′. In all line-of-sight magnetic field maps (B_L), solid (dashed) contours represent positive (negative) fields of 100, 250, 500, 1000, 1500, 2000 and 2500 G. In overlaid transverse field plots (AZ), the transverse field strength and direction are indicated by the length and orientation of the line segments. (a) Overlay of the transverse magnetic field (AZ) on contours of B_L from observations on November 2. A magnetic delta configuration is formed by the intrusion of the negative-polarity sunspot into the positive-polarity field just to the east of the large positive-polarity spot. Analysis of the line segments representing the transverse field that are overlaid on the contours of B_L reveals a generally potential-appearing field, aligned more or less directly from the positive center to the negative portion of the delta. (b) Overlay of AZ on contours of B_L from observations on November 3. Note the growth of the positive fields to the north of the delta. (c) AZ/B overlays for November 4. Growth of the fields continues, but the field orientation remains generally potential in appearance. (d) B_L field on November 5. (e) Overlay of AZ and B_L for November 5. Only the high B_L field contours from panel d have been depicted in order to make more visible the highly-sheared transverse field along the neutral line. The increase in field strengths and gradients can be seen from comparisons of panels d with panels a, b and c, where the contour levels are all the same. (f) Contours of the vertical component of the electric current density (Jz) for November 5 (see Section 1.3.3.1.). Positive (negative) Jz values of 150, 200 and 250 × 10^{-4} A m^{-2} are depicted by solid (dashed) curves. The neutral lines of panel d have been superposed to aid in orientation.

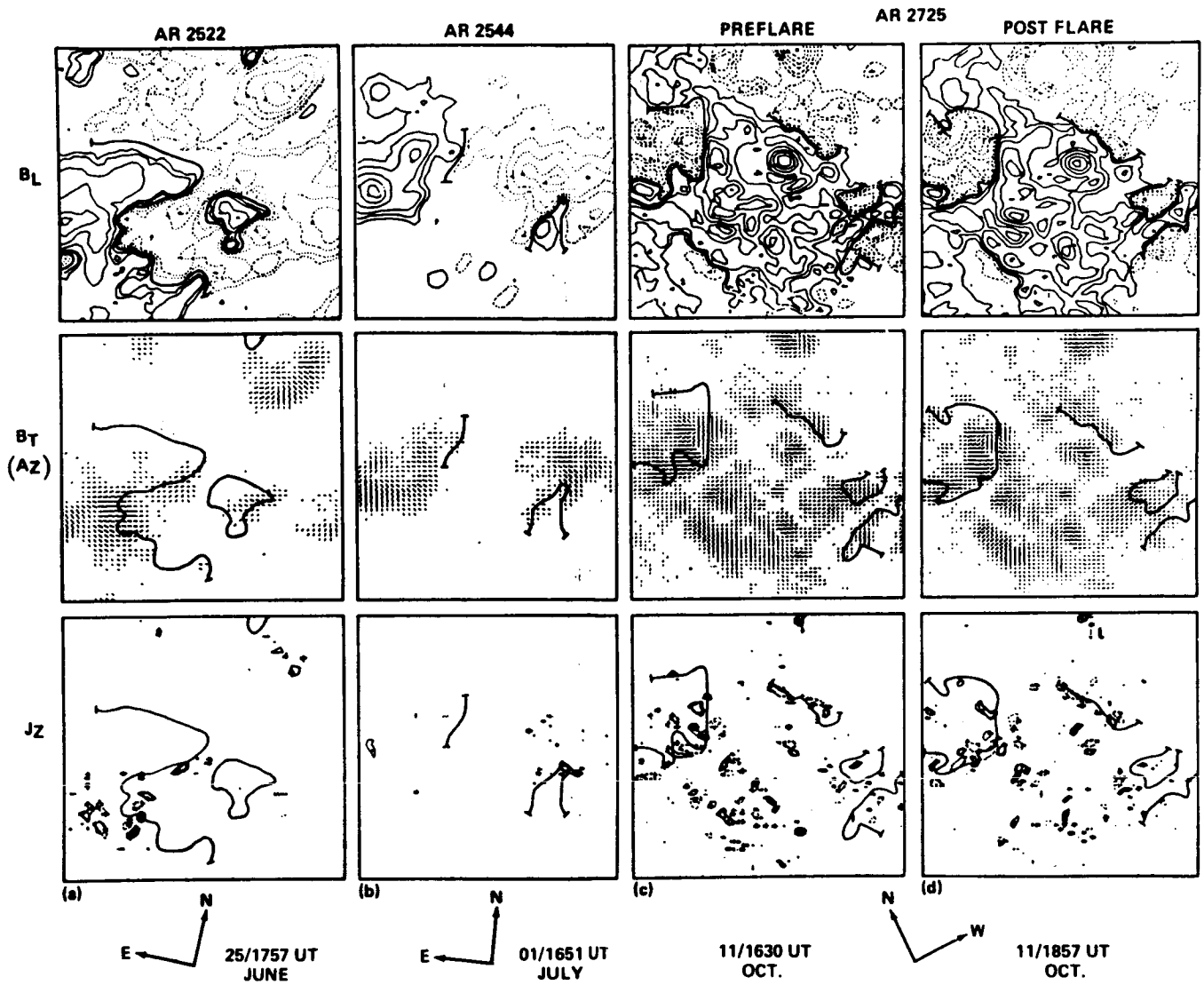

Figure 1.3.3 Vector magnetic fields and electric currents for active regions selected for study by the Preflare Group. The panels in the top row depict the longitudinal magnetic field B_L wherein positive (negative) fields are represented by solid (dashed) contours; contour levels are 100, 250, 500, 1000, 1500 and 2000 G. Panels in the center row show the transverse field B_T depicted as line segments whose length and direction represent the strength and orientation of the transverse component; the magnetic neutral lines are superposed. The bottom row depicts the corresponding vertical electric current densities with the neutral line overlaid in bold lines; contour levels are 150, 200, and 250 $\times$ 10^{-4} A m^{-2}. (a) Data for AR 2522 on June 25, 1980. Only weak shear is seen along the convoluted neutral line in the area of the southern boundary of the large intruding peninsula of positive polarity near the center of the field-of-view (2.1′ $\times$ 2.1′). (b) Data for AR 2544 on July 1, 1980. This region was born near central meridian on June 28, but it developed only minor magnetic complexity in the area of the isolated positive spot to the south of the leading negative spot. Field-of-view is 2.1′ $\times$ 2.1′. (c) Preflare data for AR 2725 on October 11, 1980. Significant magnetic shear is seen along the neutral line that lies to the left of the center of the magnetogram, with additional, weaker shear found along the neutral line lying above and to the right of center. The field-of-view is 2.5′ $\times$ 2.5′. (d) Postflare data for AR 2725 on October 11, 1980. The IB/C7 flare, which occurred about midway in time between the two megnetograms (c and d), coincided with the area of most significant shear. At 17:42 UT, near frame maximum, the X-ray loops appeared centered over the north-south portion of the neutral line to the left of center. The field-of-view is the same as in c.

examination of the transverse field reveals only weak shear along the convoluted neutral line. The region produced numerous minor flares, with a few class M events during its disk passage.

But the third region AR 2544 (column b) proved to be anomalous. It produced only a few flares, but there was a rash of activity on June 30th, including an M1, and a major flare (X2) on July 1st, the day of the illustrated magnetogram. From the magnetic data, there appears to be only the minor complexity of the isolated positive spot intruding into the southern portion of the leading negative polarity, and there is clearly no evidence of strong or extensive shear.

In another anomalous example, the active region complex composed of NOAA active regions 2516, 2517 and 2519 produced very little flare activity along the segments of the magnetic neutral line which showed the most evidence of shear in the transition region (Athay *et al.*, 1984). The flares that did occur were mainly associated with emerging flux regions. The magnetic shear was either "rather stable" or did not generate sufficient free energy to fuel a flare.

However, an important factor may be the overall configuration of the magnetic field from the photosphere through the transition region. For the relatively inactive June complex, Athay *et al.* (1984) inferred the configuration of the magnetic field from observations of fluid flows in the transition region. They found that the extreme velocity shears in the transition region diminished greatly at the photosphere. If the fluid flow follows magnetic lines of force, this result seems to indicate that the magnetic shear also decreased from the transition region into the photosphere (see Section 1.3.4.2). Such a configuration appears to be exactly opposite to that reported by Krall *et al.* (1982) for a flare-productive active region where the flares occurred at the sites of greatest shear (Hagyard *et al.*, 1984a) as deduced from photospheric observations with the MSFC vector magnetograph. Investigating the field configuration at higher levels, Krall *et al.* found that the short fibrils seen in Hα aligned with the sheared photospheric field, whereas the orientation of the longer, and presumably higher, fibrils was more or less normal to the magnetic neutral line, a configuration indicative of less shear. Thus, the overall structure of the magnetic field in this more active region was one of decreasing shear in going from the photosphere up into the lower corona.

1.3.2.3 Formation of Magnetic Shear

There is good observational evidence that magnetic shear forms as the result of sunspot motions. Two particularly good examples correlating sunspot motions with the development of photospheric magnetic shear and subsequent flare activity were unveiled in the course of the workshop. The first was the active region of early April 1980, Boulder number 2372. Born on the solar disk early on April 4, it produced many flares during its period of growth and development. Observations made at the Yunnan Observatory on April 5 from 00:50 to 09:15 UT showed the rapid development of three sunspots through the coalescence of several smaller spots (Hoyng *et al.*, 1982). The motions of the smaller sunspots were grouped into three sectors, with the spots in each sector converging and coalescing into one of the three major sunspots seen on the 6th. Since these motions involved spots of different magnetic polarities, stretching and/or shearing of the inter-connecting fields probably occurred, with energy buildup taking place in the process. Sunspot motions occurred through the 6th, as inferred from MSFC white-light photographs and the magnetic field changes seen in Figure 1.3.4. These motions continued until 19:00 UT on the 7th, whereafter no significant motions were observed. In an extensive study of this active region, Krall *et al.* (1982) found that these spot motions produced significant shear in the magnetic field with resulting flare activity in the region. This can be seen in Figure 1.3.5 which shows the first large flare on the 5th, and the most intense one, on the 6th, both occurring at the locations of the isolated positive spot and the eastward-moving negative spot. Krall *et al.* related the formation of magnetic shear to the spot motions using the observed orientations of the transverse fields as shown in Figure 1.3.6. These observations confirm that the transverse magnetic field evolved from a slightly sheared configuration on the 5th (Figure 1.3.6a) into a strongly sheared one on the 6th (Figure 1.3.6b), which then relaxed on the 7th (Figure 1.3.6c) as the sunspot motions ceased. Following this apparent relaxation of the field, the high frequency of flares which occurred through the 7th ceased, and little significant flaring was produced on the 8th and 9th.

The second example was provided by G. Chapman, who presented filtergrams, spectroheliograms and magnetograms showing the buildup of stressed magnetic fields through both rotational and translational motions of a large sunspot in conjunction with a satellite spot of opposite polarity in close proximity to the main spot. Observations of AR 2530 were obtained at the San Fernando Observatory (SFO) for approximately 9½ hours on June 24, 1980.

They showed that during this interval, the leading sunspot of this region rotated and deformed substantially from a round to a U-shape. The satellite spot of opposite polarity was adjacent to one edge of the evolving leader spot; the satellite remained intact until the following day despite the drastic changes of its larger companion. The deformations increased the magnetic gradients in the area of the satellite spot. Major flaring took place while the compression and twisting of the magnetic fields were occurring, rather than after the maximum deformation had been reached. This suggests that the rate of change in the stressing of the magnetic field was more a factor in the flare activity than the sheared topology of the field. In addition, the persistence of the satellite spot following the large flare suggests that magnetic shear between the satellite and main sunspot, rather than the high

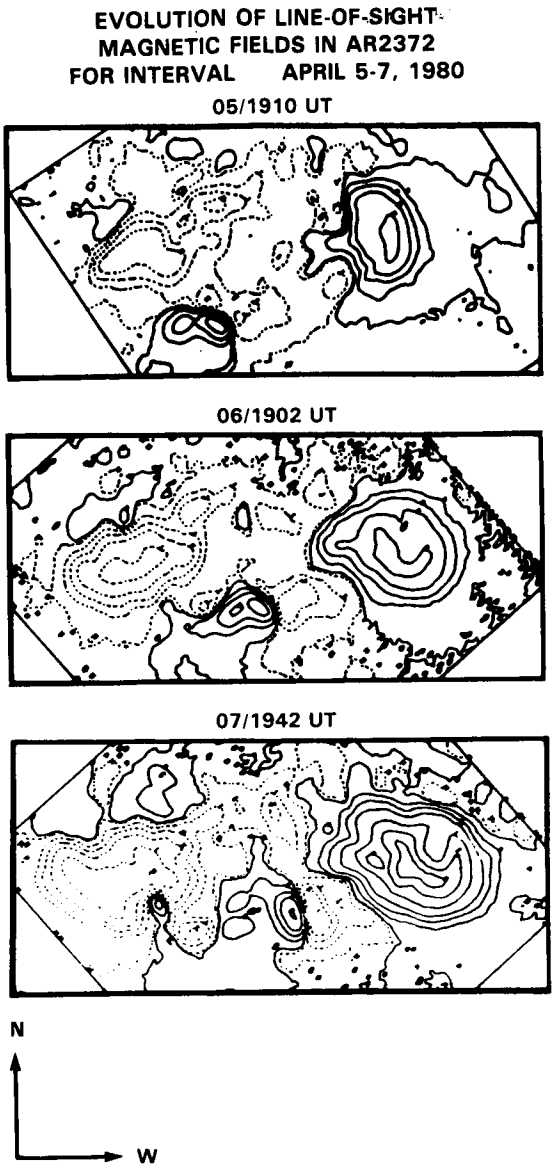

Figure 1.3.4 Evolution of the line-of-sight magnetic field in AR 2372 for April 5-7. In all panels the contours represent positive (solid curves) and negative (dashed curves) magnetic field polarities. The panels are portions of 5′ × 5′ fields-of-view. Top panel: the sunspot motions occur in the area of the internal magnetic dipole lying to the south of the large following-polarity (negative) sunspot that is located to the left of the center in this panel. Middle panel: from the 5th to the 6th, the isolated positive-polarity spot moved westward toward the large, leading-polarity (positive) spot at ≈ 160 m s^{-1}, while the adjacent negative spot, initially observed just to the north of the isolated positive spot, moved eastward toward the large, following-polarity spot at ≈ 60 m s^{-1}. Bottom panel: the field configuration on the 7th after the major spot motions had ceased.

field gradient associated with the satellite spot, was the more important factor for the flare.

There are mechanisms other than spot motions that might produce sheared magnetic fields. Newly-emerged flux can produce such complex magnetic configurations as "kinky" neutral lines, satellite spots, and δ-configurations, all recognized as correlating positively with the frequent occurrence of flares. The statistical studies of J.B. Smith, Jr. (private communication) and Patty and Hagyard (1984a) show that both kinky neutral lines and δ-spots associated with flare activity are areas of sheared magnetic fields. Sturrock (1983, FBS Study Work Group on magnetic shear, Big Bear Solar Observatory) has suggested that in the process of flux emergence the upflows that bring the field to the surface may shear the emerging field due to the coriolis force. Athay *et al.* (1984) proposed that the sheared magnetic and velocity configurations they observed in the transition region might be produced by two coherent masses of gas of opposing magnetic polarity converging in the stably stratified layers of the solar atmosphere. This suggestion that shear is produced by two converging eddies is based on analogy with shear in the terrestrial atmosphere. Tang (1983) argues that shear also is produced when originally unconnected sunspots of opposite polarity move past each other. Flux cancellation and submergence probably occurs at the neutral lines in active regions (Rabin *et al.*, 1984), and processes may contribute in the formation of sheared magnetic fields.

1.3.2.4 The Role of Magnetic Shear in the Flare Process

However magnetic shear is produced, its existence and association with flares have been directly demonstrated. Questions then arise as to the exact nature of this association, the role of magnetic shear in the buildup of flare energy, and the triggering and eruption of the flare when a critical value of shear is attained.

In a study of magnetic shear, Wu *et al.* (1984) used a self-consistent magnetohydrodynamic (MHD) model of shearing magnetic loops to investigate the magnetic energy buildup in AR 2372 the period April 5-7. Wu *et al.* argued that the evolution of the field observed between the opposing poles of the bipolar region was consistent with a gradual, relative displacement of the bipolar footpoints which occurred during the period April 5-6 (see Figure 1.3.6). The separation of the footpoints of the loops, the maximum footpoint field strength, and the average separation speed of the two spots were all determined from the observational data and used as the initial boundary conditions for an MHD model of an arcade of magnetic loops whose footpoints undergo shearing motions in opposite directions.

Calculations were performed for two different initial configurations of this field: a potential and a force-free field. The photospheric shearing motion of the footpoints of the magnetic arcade was simulated by imposing antiparallel mo-

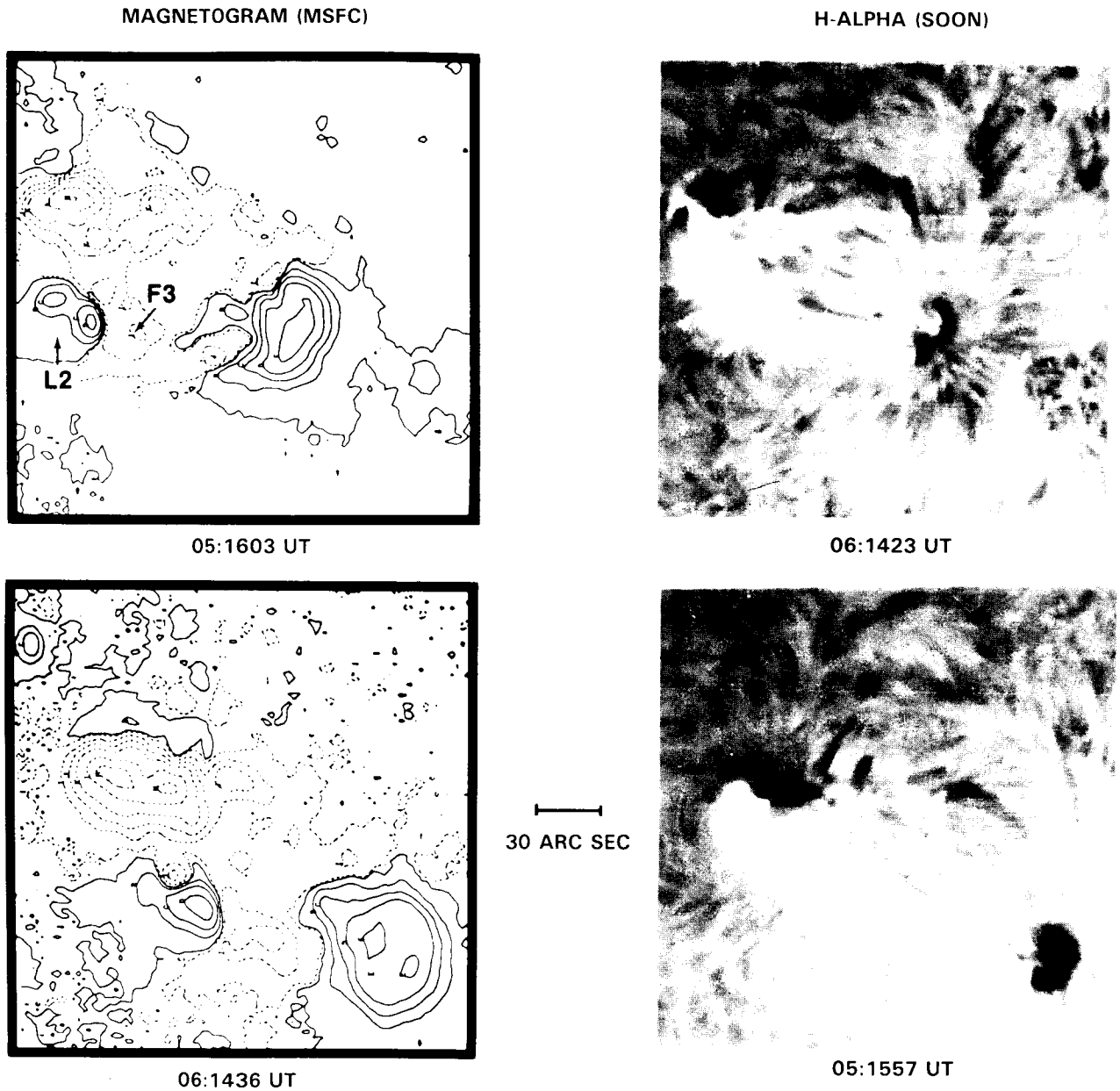

Figure 1.3.5 Magnetograms and H-alpha images for two flares in AR 2372. The left-hand panels depict the observed line-of-sight magnetic field, using the format of figure 3.4. The right-hand panels show H-alpha images from the SOON system for the flares of April 5th (a IB/M5 at 15:57 UT) and April 6th (a 1B/X2 at 14:23). Comparisons of the flare locations with the magnetograms show that both flares occurred in the area of the bipole where significant spot motions were taking place. The fields-of-view are 5′ × 5′.

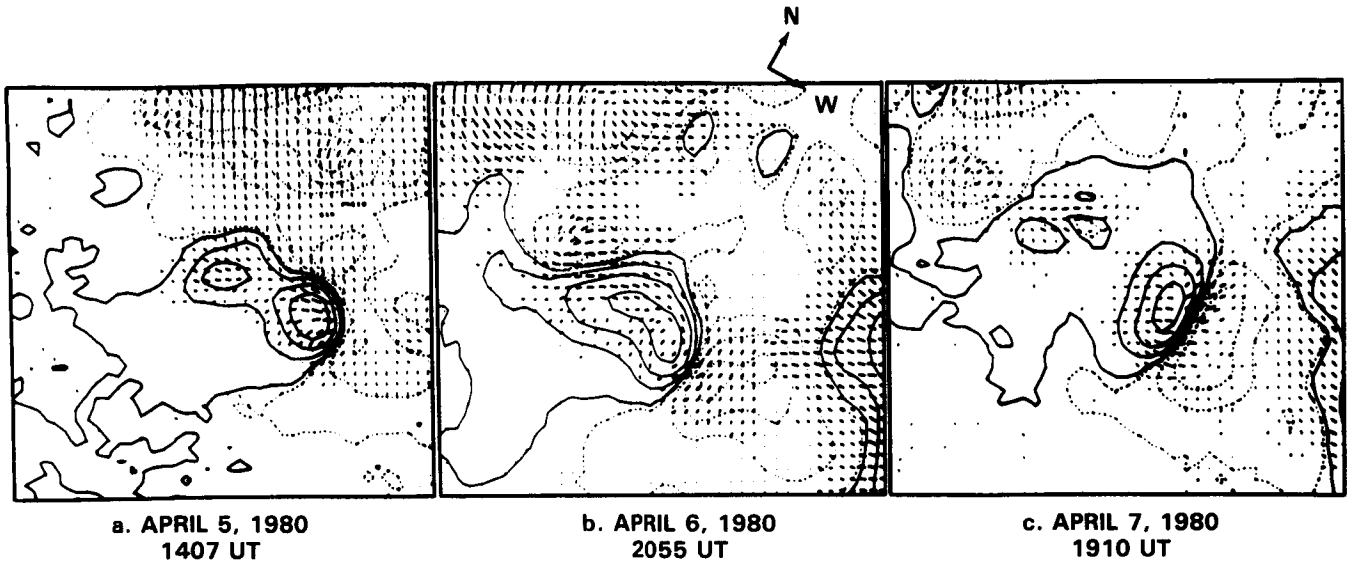

Figure 1.3.6 Evolution of the transverse magnetic field of AR 2372. All panels show the observed line-of-sight magnetic field as solid (positive) and dashed (negative) contours with the transverse field superposed as line segments whose length and direction indicate the strength and orientation of the transverse field. The fields-of-view are 167′ × 167′ and represent blowups of the bipolar region in Figure 3.5. (a) At 14:07 UT on April 5 (shortly before the flare shown in Figure 3.5), the transverse field east of the isolated positive spot was oriented perpendicular to the neutral line. However, to the north and west of this spot, some alignment with the neutral line was seen, implying the presence of shear in the field. (b) By 20:55 UT on the 6th, during the period of spot motion, the strong transverse fields were sheared along most of the neutral line, indicating significant energy storage. (c) Following cessation of spot motion, the shear in the transverse field was less pronounced as observed on the 7th at 19:10 UT.

tions on the footpoints on opposite sides of the neutral line. The magnitude of the velocities varied sinusoidally with distance from the neutral line (axis of the arcade). The self-consistent solutions from this model provided numerical values for the magnetic field, velocity, density, temperature, and pressure as functions of two spatial dimensions and time.

Figure 1.3.7 shows a typical result from this calculation; the different energy modes are shown as functions of time as the photospheric shearing motions proceed for the case of an initial potential magnetic field. The magnetic energy buildup clearly dominates, and its growth rate becomes constant after a short interval, while the interaction among the other modes of energy becomes insignificant. Results obtained for different initial values of the parameters are summarized in Table 1.3.1, which gives the energy growth rates in erg day^{-1} per km of arcade length. For parameter values typical of the observed conditions, where magnetic energy density dominated the plasma thermal energy density at the photosphere by a factor of 10, i.e., $\beta_0 = 0.1$, and where the maximum shearing velocity was 0.1 km s^{-1}, the rates of energy buildup are $2 \times 10^{30-31}$ and $1 \times 10^{31-32}$ erg day^{-1} for initially potential and force-free fields, respectively, taking arcade lengths of 10^{4-5} km. These values are consistent with the observed flare output rates that were estimated by Krall *et al.* (1982) to be 2×10^{31} erg day^{-1}. Examination of the spatial distributions of magnetic energy showed that the highest concentration of magnetic energy was located near the neutral line, with the concentration being more pronounced in the case of the pre-sheared (force-free) field configuration.

Critical Value of Shear — The preceding studies demonstrate that magnetic energy sufficient to fuel solar flares is accumulated as a result of increased shear in the magnetic field, with the growth rate of magnetic energy roughly proportional to the shearing speed, to the length of the affected neutral line, and approximately inversely proportional to the initial value of the plasma parameter β_0. The next problem, then, is to determine the mechanism by which this free energy is suddenly released in the form of a solar flare. In the context of the smooth buildup of magnetic energy through increasingly greater shear in the field, it is tempting to think in terms of a "critical" value of this shear which,

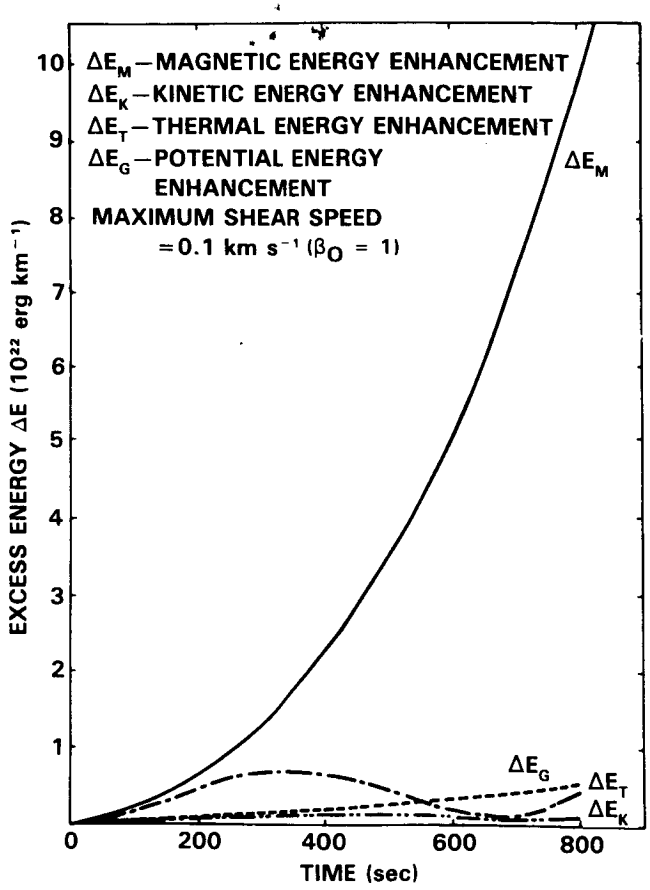

Figure 1.3.7 Magnetic energy buildup through shearing of magnetic fields: results of an MHD model calculation. The calculation models an arcade of magnetic loops whose footpoints on opposite sides of a magnetic neutral line undergo shearing motions in opposite directions. The excess (above that at time t = 0) magnetic, kinetic, thermal, and potential energies are shown as functions of time for an initially unsheared magnetic field configuration. Note that the buildup of magnetic energy dominates and is approximately an order of magnitude greater than the kinetic, thermal and potential energy modes.

when exceeded, triggers the release of energy at these sites of excess shear. Such a concept has been proposed by several theorists (Barnes and Sturrock, 1972; Low, 1977a, 1977b; Birn *et al.*, 1978; Hood and Priest, 1980). The shear in their static models is successively increased until a critical value is reached, after which there are no equilibrium solutions; this critical point has been interpreted as the threshold for the onset of a flare.

Recently, observational evidence for the existence of such a critical shear has been reported by Hagyard *et al.* (1984a). In their study, these authors analyzed the degree of shear along the neutral line of AR 2372 at a time midway through its early period of flare activity, April 5-7, 1980. They defined the degree of shear, $\Delta\phi$, to be given by the difference at the photosphere between the azimuths of a potential field and the observed field, where the potential field satisfies the boundary conditions provided by the observed line-of-sight field; these fields are depicted in Figure 1.3.8. Using these data, the parameter $\Delta\phi$ was evaluated at 55 points along the neutral line; points 1 and 50 are designated in Figure 1.3.8b. Figures 1.3.8c and 1.3.8d show the variations of the magnitude of the transverse magnetic field (B_T) and $\Delta\phi$, respectively, along the neutral line. In Figure 1.3.8d, the *asterisks* mark points for which B_T is less than or about 100 G; there probably are substantial errors in the observed azimuth at these points, so the corresponding values of $\Delta\phi$ should be regarded with skepticism. Excluding these points, one can see in Figure 1.3.8d that the degree of shear is non-uniform along the neutral line, and has two negative maxima of values $-85°$ and $-80°$ along the segments marked A and B, respectively. In addition, from comparisons of B_T with $\Delta\phi$, these very large shears seem to occur preferentially at locations of maximum values in the transverse field strength. The authors argued that the configuration of the magnetic field at the time of the observations (21:10 on April 6) represented the most sheared state attained by the field in the period April 5-8. During the period 14:00 to 21:00 on the 6th, there were no significant changes in the observed azimuth, even though four major flares then occurred.

The sites of flare onset for the 1B/X2 flare at 14:18 UT on April 6, as inferred from the most intense chromospheric flare emissions observed in off-band Hα, were located on either side of the magnetic neutral line along the segments corresponding to A and B in Figure 1.3.8d, that is, at the sites of maximum photospheric shear. Furthermore, in a later flare for which spatially-resolved X-ray data were available (00:48 UT on April 7), the locations of soft X-ray onset were placed at A. Because the flares occurring in AR 2372 in this time period were homologous, the sites of flare onset for these two observed flares are probably representative of the sites for most of the flares during this period.

Based on these results, the authors proposed a scenario for these flares wherein continued magnetic evolution caused the field's maximum shear to exceed a critical value ($> 80 - 85°$), resulting in a flare at and above the site of maximum photospheric shear. The flare signaled a relaxation of the shear to a value somewhat smaller than the critical value, with further evolution increasing the shear above threshold, another flare, and so on. This scenario, based on observational evidence of persistently sheared fields throughout a flaring epoch, argues against the idea that relaxation of the magnetic field, due to the release of energy in the form of a flare, must proceed until the local shear is negligible. This argument gains support from the preceding analysis of Wu *et al.* (1984) who showed that energy is more efficiently

Table 1.3.1 Energy growth in erg day^{-1} per km depth

Shearing Velocity km s^{-1}	Initially Untwisted Magnetic Field		Initially Twisted Magnetic Field (A 40° Twist)
	$\beta_0 = 0.1$	$\beta_0 = 1.0$	$\beta_0 = 0.1$
0.1	1.94×10^{26}	2.07×10^{25}	1.08×10^{27}
1.0	1.3×10^{28}	2.27×10^{27}	1.12×10^{29}
20	2.66×10^{30}	3.24×10^{29}	

stored in a field that is already significantly deformed, and that this energy is more concentrated near the neutral line for such a deformed field.

1.3.3 Electric Currents in the Preflare Active Region

The presence of sheared, photospheric magnetic fields in the pre-flare state implies the existence of electric currents in the atmosphere above the photosphere in which superpotential energy is stored and subsequently released in the outbreak of a solar flare. This release of energy is generally considered to result from resistive MHD instabilities that involve currents flowing either parallel to the magnetic field or perpendicular to the field as in the case of an X-type neutral point. Thus, the concept of a critical value of magnetic shear may have its counterpart in "critical" values for these currents.

Observational data that yield information on the magnitudes and distributions of these currents provide useful constraints on their models of solar flares. The most direct measure of solar currents available comes from observations of the vector magnetic field at the photosphere, from which we can derive the vertical component (J_z) of the electric current density passing through the photosphere, using the relation $(\nabla \times B)_z = \mu_0 J_z$. Quantitative values of J_z have been estimated with an uncertainty of 25×10^{-4} Am^{-2} which is inherent in the measurement of the magnitude and azimuth of the transverse component of the magnetic field.

1.3.3.1 J_z Concentrations in Flaring Active Regions

The study by J.B. Smith, Jr. (Section 1.3.2.2) of sheared magnetic fields in active regions was extended by deLoach to include the vertical component of the photospheric electric current density, J_z. This study utilized the magnetic field data for the regions and times listed in Table 1.3.2 with notable flares. The J_z patterns shown in Figure 1.3.2f and in the bottom panels of Figure 1.3.3 correspond to the regions listed in that table. In a majority of these regions, concentrations of J_z were seen along the magnetic neutral line. Indications of additional strong currents often appeared well away from the neutral line; but most of these latter J_z features are probably artifacts of the computational techniques used to resolve the 180° ambiguity in the direction of the magnetic field's transverse component or of the small signal-to-noise ratio in umbral areas. There is a greater level of confidence in the J_z patterns calculated from the sheared transverse magnetic fields in the vicinity of the neutral line where these complications are not a factor.

With these caveats in mind, examination of the data showed that J_z concentrations exist in neutral-line regions where flaring occurs; the strength of these currents depends upon the degree of shear present in the vicinity. As discussed in Section 1.3.2.2, a notable increase in field strength and gradient took place in AR 2776 on November 5, and the transverse field directions were closely aligned along the principal neutral line. The J_z calculations for that region show strong currents in that same area, as seen in Figure 1.3.2f. In the case of AR 2725 (Figures 1.3.4c and d), in which the transverse field is highly sheared along the north-south portion of the principal neutral line, strong currents are present in those locations as well. It was also noted that the X-ray flare which took place in this region on the 11th at 17:41 UT had a loop structure that crossed, and was centered over, this area of strong shear and J_z.

The example shown for AR 2522 in Figure 1.3.4a reveals that an area of weak shear lies along the neutral line to the east. Once again the strongest currents lie in the vicinity of these same areas of the neutral line. Finally, in the example of AR 2544, a rather active region of very little magnetic complexity, the amount of shear present was weak and located near the top of the loop-shaped neutral line at the right of Figure 1.3.4b; that is also the site of the only area of significant J_z.

Examination of these and other data for J_z reveals that the existence and general behavior of the photospheric currents in flare-productive active regions are consistent with the degree of persistence and amount of shear exhibited by the transverse magnetic field along the magnetic neutral line. We infer from these observations that the somewhat stable nature of the sheared field configuration throughout the ac-

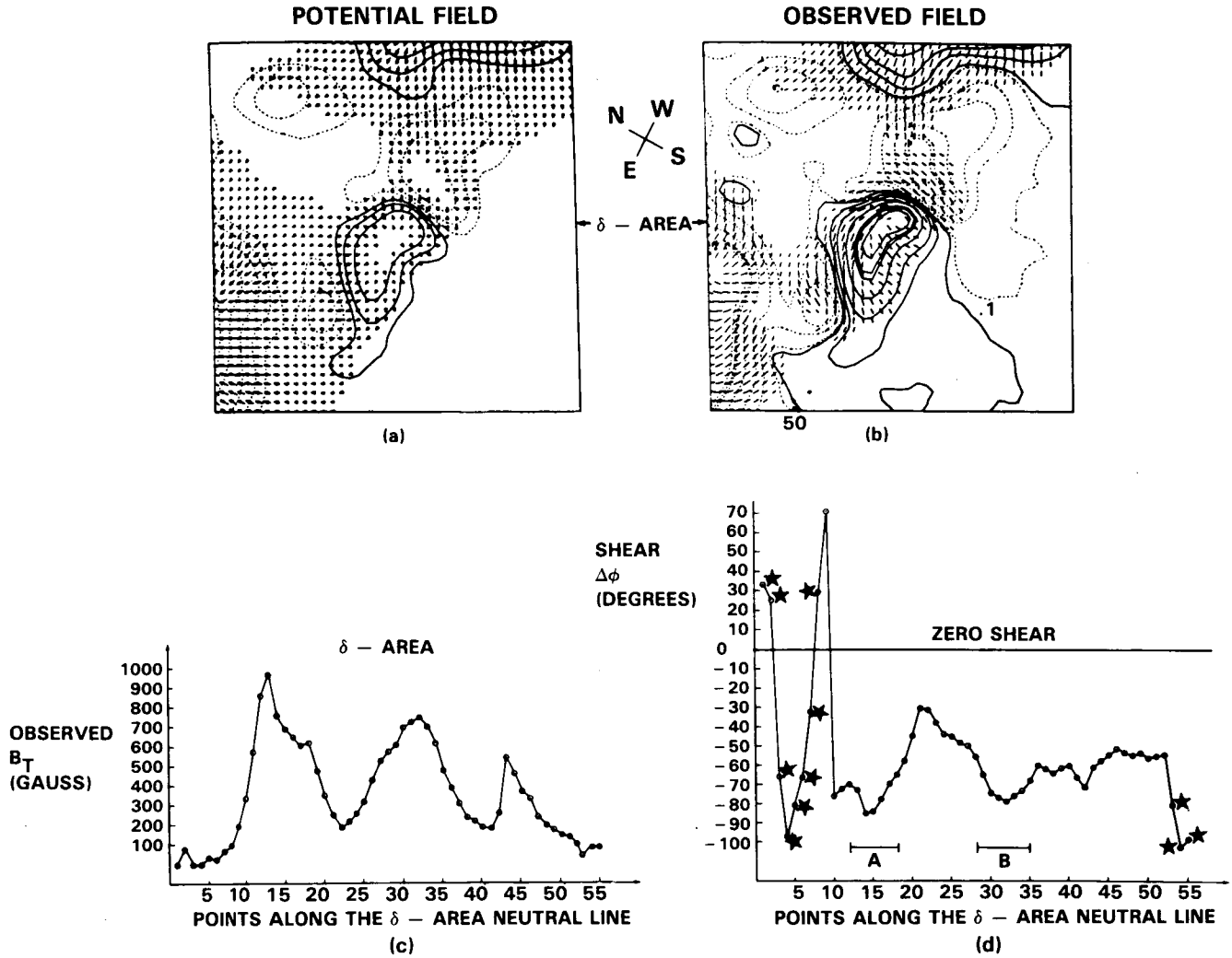

Figure 1.3.8 A quantitative evaluation of magnetic shear in AR 2372 on April 6, 1980. In the region of the small bipole lying to the southeast of the large leader sunspot in that flare-productive active region (see Figure 3.5b), the observed field is compared with a potential field in order to determine their deviations near the magnetic neutral line. (a) The potential magnetic field in the area of the bipole. The potential field was calculated from the observed line-of-sight field. Solid (dashed) curves represent positive (negative) contours of the line-of-sight magnetic field. The directed line segments represent the strength (length) and orientation (direction) of the transverse field. (b) A similar image for the observed magnetic field. In both panels the field-of-view is 1.67′ × 1.67′. (c) Variation of the magnitude of the observed transverse field along the magnetic neutral line. (d) Variation of the degree of shear along the neutral line. Points marked with an asterisk occurred in areas of very weak transverse field and thus are unreliable. The degree of shear exhibits two maxima at points "A" and "B" along the neutral line. These maxima coincide with increased values of the strength of the transverse field.

tive lives of these regions applies to J_z as well, and that the continued presence of magnetic shear and electric currents at and near flare sites indicates that further activity is likely to occur.

1.3.3.2 Correlations of J_z Concentrations with Sites of Flares

For one active region studied in detail, Hagyard *et al.* (1984b) found a strong correlation between the sites of flare knots and concentrations of J_z, thus confirming the previous work of Moreton and Severny (1968). The observations were carried out on April 6, 1980, at 21:10 UT in active region 2372 (see also section 1.3.2.4); the results are shown in Figure 1.3.9 which shows the observed magnetic field and derived electric currents. In Figure 1.3.9b, one can pick out seven compact areas of maximum J_z with $J_z \approx 0.025$ A m^{-2}; these maxima are designated by the numbered labels indicated in Figure 1.3.9b. Since the maxima at areas 1, 3,

Table 1.3.2 Date and Times (UT) of MSFC Magnetograms (B) and SMM Events (E)
Flare Precursor Matrix Study

AR 2522 JUNE 1980	AR 2544 JUNE/JULY 1980	AR 2725 OCTOBER 1980	AR 2776 NOVEMBER 1980
19 — 1839 E	30 — 2044 B	9 — 2116 B	5 — 1754 B
20 — 1722 B	30 — 2135 B	10 — 1504 B	5 — 2223 E
20 — 2025 B	30 — 2312 B	10 — 1809 B	6 — 1445 B
25 — 1550 E	1 — 1628 E	11 — 1529 B	
25 — 1757 B	1 — 1651 B	11 — 1630 B	
25 — 2156 B	1 — 2052 B	11 — 1741 E	
26 — 1410 B	1 — 2235 B	11 — 1857 B	
26 — 2130 B	2 — 1434 B	12 — 1423 B	
27 — 1402 B			
29 — 0235 E			
29 — 1041 E			

and 7 occur for only one data pixel, they should be viewed with some skepticism in comparison with the other four maxima.

These locations of maximum J_z were compared with the spatial distribution of flare intensities observed for the 1B/X2 flare that began at 14:18 UT on the 6th, about 7 hours prior (see Section 1.3.3.3 following) to the time of the J_z data. In Figure 1.3.9, the locations of the most intense Hα emissions for that flare are shown with respect to the magnetic neutral line derived from an observation of the magnetic field near the time of the flare. In addition, "A" indicates the location of onset for a flare at 00:48 UT on the 7th (4 hours after the J_z observations) as seen in soft X-ray observations from SMM (Machado *et al.*, 1983). Comparison of Figures 1.3.9b and 1.3.9c shows that the areas of enhanced J_z were approximately cospatial with the sites of flare onset.

1.3.3.3 Evolution of J_z Patterns

The sheared configuration of region AR 2372 persisted during the period of these flares on the 6th and early 7th, with no perceptible relaxation taking place following the flares (Hagyard *et al.*, 1984a). From this observation, one infers that the pattern of J_z concentrations also showed no significant changes during this particular period. However, during most of the interval April 5-7, intense and rapid magnetic evolution took place in the area of the δ configuration with significant flare eruptions. Thus, one suspects that the J_z configuration also was undergoing significant changes during this interval. To investigate this further, deLoach has studied the emergence and evolution of the J_z patterns in the δ-area of AR 2372 from April 5-7. His aim was to determine whether the patterns changed rapidly in strength and/or location, or were in fact maintained over periods long in comparison with the observed flare activity. The region history has been discussed in a previous section (1.3.2.3) and in Krall *et al.* (1982). Although the region emerged very early on 1-58 April 4, the first vector magnetic field data were not obtained until about 14:00 UT on the 5th. Thus it was not possible to see the initial emergence of a J_z pattern as the region appeared and grew on the 4th.

For the study of the evolution on the 5th, vector magnetograms obtained at five intervals between 14:00 and 19:00 UT were selected for J_z calculations; the results are summarized in Figure 1.3.10. The sheared nature of the magnetic field along the neutral line is evident in each of the panels depicting the transverse field (B_T): the azimuths are closely aligned with the neutral line. This nonpotential field configuration implies a non-zero curl in these areas and, hence, that electric currents are present. This expectation is borne out in the maps of J_z shown in the bottom panels of Figure 1.3.10. In that figure obvious changes appear in the magnitudes of the line-of-sight and transverse components of the magnetic field as well as in the azimuths near the neutral line. These might be expected because of the evolving magnetic complexity during this period, although some of the subtler changes are seeing effects. The most significant change in the transverse field occurred between the magnetograms obtained at 14:07 and 16:03 UT. This observation is especially interesting since a flare classified as 1B/M5 took place in the region at 15:54 UT. Despite its restructuring the field remained highly sheared at the neutral line. Furthermore, the site of the strongest current density, which was seen in the earliest observation at 14:07 UT, persisted in its location relative to the neutral line throughout the series of observations, that is, just above the "dip" in the neutral line and extending along the left section of that part of the neutral line.

To extend the study of the evolution of J_z in this active region, deLoach used the maps of J_z generated by Krall *et al.* (1982) for April 6 and 7; these show that the sites of strongest current density on the 6th remained along the neu-

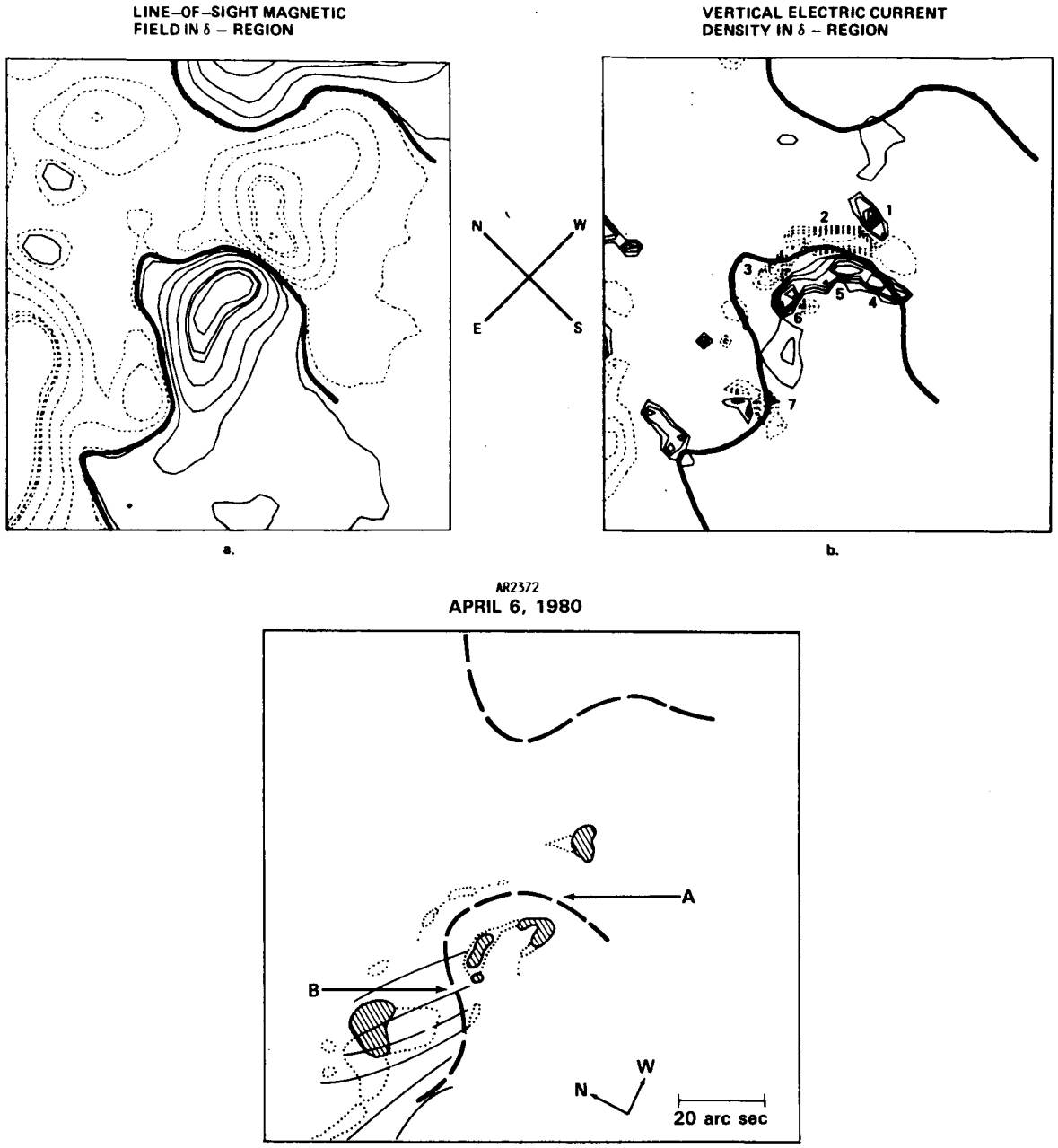

Figure 1.3.9 Concentrations of electric currents at flare sites in AR 2372 on April 6, 1980. (a) The line-of-sight magnetic field observed at 21:10 UT in the area of the magnetic bipole lying to the southeast of the leader spot (see also Figure 3.5b). This area was the site of most of the early flares in AR 2372. Solid (dashed) curves represent positive (negative) contours of the field. (b) Calculated vertical electric current densities (J_z) for the same field-of-view (1.67′ × 1.67′) as panel a. The heavy solid curve delineates the magnetic neutral line in panel a to aid in orientation. Five contour levels of J_z are shown in the panel: 50, 100, 150, 200, and 250 × 10^{-4} A m^{-2}; solid (dashed contours) represent positive (negative) values of J_z, with "positive" indicating a J_z flowing upward out of the photosphere. Note the seven areas of concentrated maxima of J_z. (c) Locations of flare intensities in AR 2372 for the IB/X2 flare at 14:18 UT on April 6, 1980. The 2′ × 2′ field-of-view of this figure is centered on the bipole area of Figure 1.3.14a, and the heavy dashed curves locate the two segments of the neutral line corresponding to those shown in Figure 1.3.14. The hatched regions show the areas of most intense off-band emission, while the dots outline areas of fainter emission. The loops sketched at "B" are inferred from the emission seen at line center and ± 0.4 Å in Hα. The area designated by "A" is explained in the text.

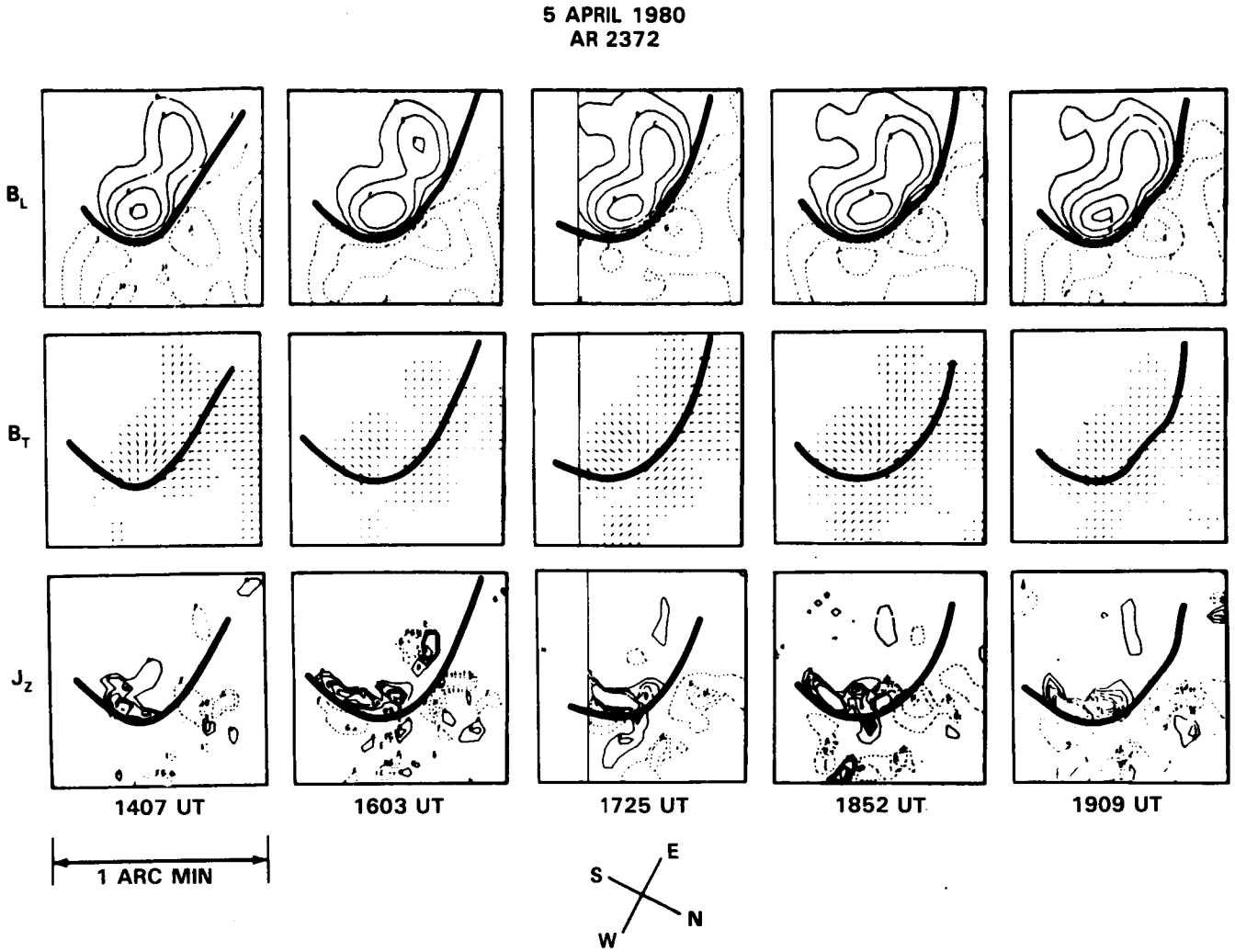

Figure 1.3.10 Evolution of magnetic shear and electric currents in AR 2372 on April 5, 1980. The top row of panels depicts the line-of-sight magnetic field (B_L) at different times in the area of the small bipolar region lying to the southeast of the main leader spot of AR 2372 (see Figure 1.3.5a). Positive (negative) fields are depicted by solid (dashed) countours; the heavy, solid curve denotes the magnetic neutral line. The middle panels show the observed transverse field (B_T) with the neutral line superposed. The line segments represent in length and direction the strength and orientation of the transverse magnetic field. The bottom row of panels shows the derived vertical electric current densities J_z, again with the magnetic neutral line superposed. The contour levels denote positive (solid lines) and negative (dashed lines) values of J_z from 50 to 250 $\times$ 10^{-4} A m^{-2}, in increments of 50. All panels are approximately 1′ $\times$ 1′ in size.

tral line, with the primary maximum still located in its western "dip" but migrated westward along with the isolated positive polarity. On April 7th, although still present, the J_z maxima are less clearly defined above the background noise.

Throughout the period studied (April 5-7), the persistent positive J_z concentration is situated in approximately the same location relative to the neutral line. However, the more notable negative J_z areas seem to shift. On the 5th, the primary negative concentration of J_z is located north of the neutral line, coincident with the negative polarity region seen in the panels of the line-of-sight magnetic field (B_L) in Figure 1.3.10 (April 5th). This suggests that the electric currents are flowing along force-free like paths that connect the positive and negative magnetic polarities. From the 5th to the 7th, significant proper motion of the spots associated with these two fields was observed. The changes in the current distributions are consistent with these magnetic changes; as the fields and currents restructure, the currents still flow across the neutral line.

1.3.3.4 J_z Correlations with Preflare Brightenings

Observations with the SMM/UVSP instrument have revealed numerous intensity enhancements in various bright

points in an active region prior to a flare (Cheng *et al.*, 1982). Studies show that these preflare bright points are sometimes, but not always, associated with the UV flare kernels. For example, for the flare on April 8, 1980, at 03:03 UT in AR 2372, Cheng *et al.* inferred that four UV bright points observed prior to the flare were footpoints of two loops crossing the magnetic neutral line; the ensuing flare occurred in one of these preexisting loops. To investigate the source of these preflare UV brightenings deLoach *et al.* (1984) have compared distributions of vertical electric current density, J_z, with UV spectroheliograms. If ohmic heating from the electric current is a significant contributor to these brightenings, these comparisons should show that sites of maximum J_z underlie areas of UV enhancements.

The active region chosen for the study was, again, AR 2372, for the period April 6-7, 1980. Two series of UV spectroheliograms were used, one in Lyα (1216 Å) and the other in N V (1239 Å). The complete series of Lyα and N V spectroheliograms indicate that the region showed persistent internal structure with preferentially bright and dark areas. In addition, the area of strongest J_z maintained its pattern within the δ-region during the period covered by the UV data. When the J_z and UV data were spatially registered, the maximum concentration of J_z fell in an area that was persistently enhanced in the Lyα/N V series.

While this result encourages the view that these brightenings are due to ohmic heating, there is no simple relation between the measured J_z and the heating. For example, there were other areas of enhanced UV emission with no cospatial current at the level of the lowest J_z value measurable. Moreover, the measured J_z maximum of 0.01 A m^{-2} would supply only about 0.1% of the average Lyα flux ($\approx 10^6$ erg cm^{-1} sec^{-1}) radiated from active regions. deLoach *et al.* concluded that although resistive heating may be important in the transition region, the currents responsible for the heating are largely unresolved in the measurements of their study ($\approx$ 5 arc sec resolution). This conclusion is substantiated by recent work of Rabin and Moore (1984), who suggest that the lower transition region is heated by filamentary, fine-scale electric currents flowing along the magnetic field.

1.3.3.5 Stochastic Joule Heating

In addition to these preflare UV brightenings, it appears that a broad range of smaller-amplitude brightenings are present in most active regions, according to the results of a study by Porter, Toomre and Gebbie (1984) reported at the workshop. Using observations obtained with the UVSP instrument, they found frequent and rapid fluctuations in Si IV and O IV line emission at sites of enhanced intensity within an active region. These brightenings were smaller in amplitude than the UV bursts that have been studied in some detail through observations from the OSO-8 satellite in the C IV and Si IV spectral lines (e.g., Lites and Hansen, 1977; Athay *et al.*, 1980).

The observations reported by Porter *et al.* (1984) were carried out during seven consecutive orbits of the SMM satellite on October 27 and 28, 1980, in Active Region 2744. Large spatial rasters were performed intermittently to locate the brightest pixel in the region. Subsequent to this, the Si IV and O IV counts in the brightest pixel were measured 1500 times with 0.08 s temporal resolution. 3″ × 3″ and 4″ × 4″ entrance slits were used. A total of 67 such sequences was obtained, covering several bright points in the region.

Though the nature of the experiment was to wander from brightest point to brightest point throughout the active region, the pointing did return a number of times to a few consistently bright points. In Figure 1.3.11, the data are shown for one of the brightest sites during the first two orbits on the 27th; this point was perhaps a footpoint of a loop that flared at 02:24 UT on the 28th. Many of the more rapid intensity variations in time were due to small-amplitude jitter in the satellite pointing. By comparing their observations with satellite-pointing data, the authors attempted to remove these effects. The relatively smooth curves drawn through the data points represent their best estimates of the actual solar output. From these and similar high time-resolution observations of bright points in this active region, the authors showed that significant increases in Si IV intensity occurred almost continually on time scales of 10 to 60 s. The intensity enhancement during the brightenings was commonly 20 to 100%, and sometimes larger. These brightenings were present throughout the period of observation, and were so prevalent as to be found in about two-thirds of the selected observing intervals. The analysis of pointing errors leads to an estimate of the possible size of the bright elements as 1″ or less.

Evidently, the spectrum of heating responses in the transition region extends from flares and the large amplitude bursts down to the smaller, and usually short-lived (20 s to 60 s), brightenings reported in this study. The transition region is apparently subjected to a variety of heating events on a broad range of spatial and temporal scales. The timing for these smaller events is compatible with an almost instantaneous local heating within the transition region followed by radiative cooling.

1.3.4 Characterization of the Preflare Velocity Field

Of equal importance to sunspot motions in characterizing the preflare state are the Doppler velocity patterns that are observed in active regions. These cover the spectrum from filament activation and eruption, surges, and preflare mass ejections to the predominantly horizontal shearing patterns that are suggestive of cyclonic motions in the photospheric areas where flares occur. For example, some of the most easily recognizable flare precursors are the distinct Doppler patterns observed in the ascending phase of erupt-

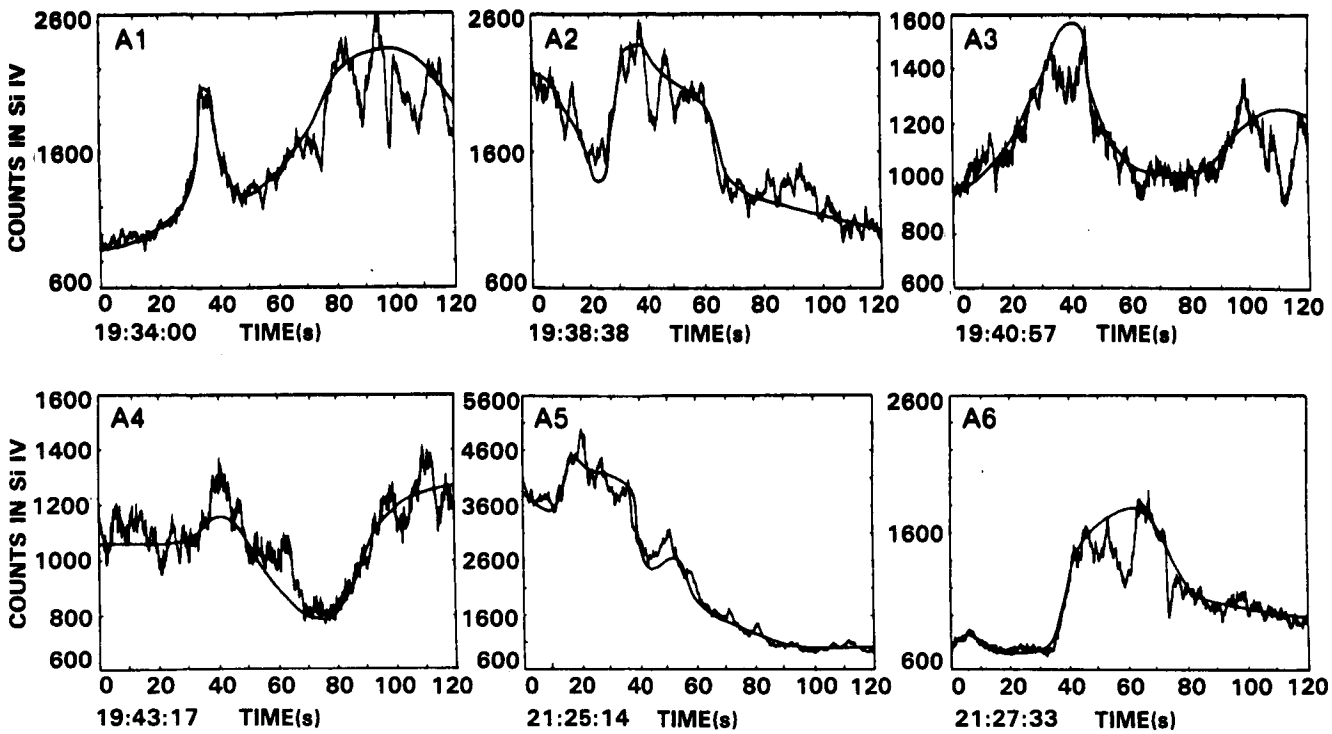

Figure 1.3.11 Rapid variations in time of Si IV λ1394 line emission observed at a persistently bright point in the active region AR 2744. Shown are results from six observing intervals each lasting 120 s; indicated are counts per sampling interval of 0.08 s. Starting times of each sequence on October 27, 1980, are indicated at the lower left. Smoother curves represent estimated true solar output; correction has been made for effects of satellite pointing variations on measured line intensity. Many rapid brightenings with lifetimes of 20 s to 60 s are present.

ing filaments (Martin, 1980). Furthermore, detailed studies of photospheric velocity fields in active regions show that flares tend to be associated with complex velocity patterns (e.g., Martres *et al.*, 1971). Harvey and Harvey (1976) reported that flares seem to occur in areas of strong horizontal velocity shear along the magnetic polarity-inversion line. They concluded that the velocity field is at least as significant as the magnetic field in the flare-buildup process, and urged that equal emphasis be placed on the study of the velocity field. During the SMM observing period in 1980, this counsel initiated many coordinated observing programs in which ground-based Doppler measurements were obtained in conjunction with observations of transition-region velocities using the UVSP instrument. In the following sections we report on results of those observations that pertain to the preflare active region.

1.3.4.1 Preflare Ejecta

During SMM, the Meudon group, represented in the Preflare Group by Schmieder and Martres, observed many surges in their investigation of the flare-buildup process. They were specifically interested in determining whether surges are produced by the same mechanism(s) as flares. They carried out several programs in conjunction with UVSP observations to define the geometrical, thermal and dynamical characteristics of surges (Schmieder *et al.*, 1983).

In one of these programs, they obtained simultaneous ground-based Hα and UVSP C IV observations of recurrent surging in an active region prior to a period of flare activity. The active region (AR 1646) was observed on September 1, 1980, during the time period 12:30-14:08 UT, near disk center. This region developed as a new active center on August 28; there followed a complex evolution over the next few days with a new dipole emerging to the east of the initial one on the 29th (Figure 1.3.12). The new preceding spot increased in size during the 31st and began to move toward the first preceding spot with a velocity of 0.1 km s^{-1}. This motion led to a compression of the following (inverse polarity) spots between the two preceding spots and caused recurrent ejections of matter on September 1 with time intervals of about 10 minutes. Frequent but minor flaring also occurred on the 1st, beginning with a SN/C3 event at 14:08 UT and ending at 22:06.

The Multi-Channel Subtractive Double Pass-Spectrograph (MSDP) in the solar tower of Meudon provided two-dimensional observations of velocities and intensities in the Hα spectral line with a spatial resolution of 1″ × 1″ and

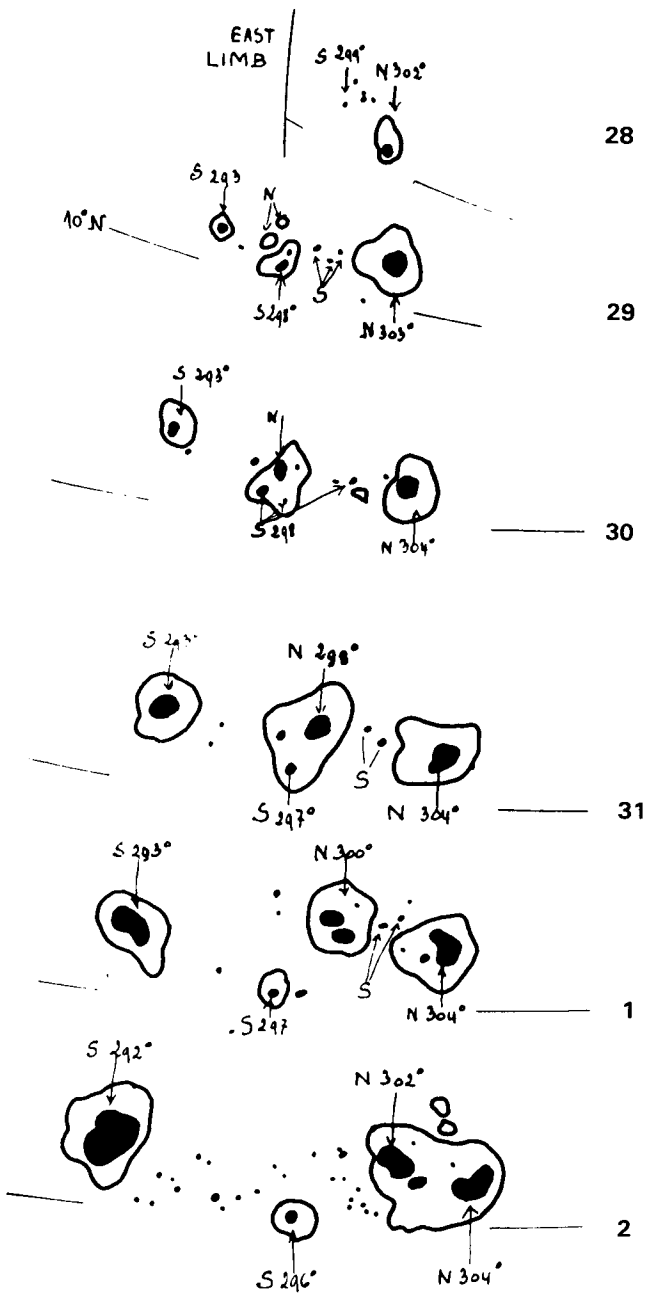

Figure 1.3.12 Evolution of AR 2646 from August 28 to September 2, 1980. The small south (S) polarity spots that were compressed between the larger, north (N) polarity spots can be seen just to the left of the leading (rightward) N-spot on the 31st.

a repetition rate of one minute. The UVSP provided a dopplergram and an intensity map in the C IV (1548 A) line over a 4′ × 4′ field, followed by a set of 24 intensity maps with a reduced field of 2′ × 2′ with spatial resolution of 3″ × 3″ which focussed on the surge event.

The intensity maps in both Hα and C IV showed recurrent maxima in brightness of the facula, but the brightenings in C IV tended to occur a few minutes prior to those in Hα. Three surge events were observed during the time period 12:32-13:15 UT. In Figure 1.3.13, the Hα velocities and intensities are shown for times near the beginning and end of the first event. The surging is clearly located between the two sunspots, along an axis perpendicular to the line joining these spots. The intensity and velocity in the transition region near the beginning of the first surge show that the C IV brightness is elongated in the same direction as the Hα emission but with a slightly greater extension. Only one UV velocity map was obtained for the first surge, at 12:32 UT. This showed upward velocities of 30 km s^{-1} and a more extended (> 2′) velocity structure than the one seen in Hα (< 1′). The C IV velocity structure also is more extended than the emission structure seen in C IV.

The time evolution of the surge was obtained from the sequence of MSDP Hα data. The brightening of the facula occurred a few minutes before the maximum extension and velocity of the absorbing feature at 12:36 UT. The redshifted area, which initially corresponded to the emission feature, progressively enveloped all of the absorbing material. The horizontal velocity along the axis of the surge was derived from the position of the absorbing matter and found to be 60 km s^{-1}.

In order to interpret the Hα data in terms of radial velocities, the Hα profiles must be carefully studied. In their interpretation, Schmieder *et al.* (1984) proposed a "cloud model" to represent the absorbing feature and considered the measured line profiles to be a convolution of two profiles corresponding to the cloud overlying the chromosphere. The observed temporal behavior of the spectra was consistent with a cloud whose velocity reversed direction. Radial velocities were evaluated to be 25-30 km s^{-1} in the ascending phase of the ejection, and 40 km s^{-1} in the descending phase.

Analysis of the complete set of data indicated that recurrent ejecta lasting 10 minutes occurred on September 1 with intervals of about 20 minutes. The observations were consistent with the following scenario. A loop emerging from the brightened facula was compressed by the two merging sunspots. In the first phase, the cold material visible in Hα followed the field lines of this loop with motions upward from the feet. However, the kinetic energy of the material was not sufficient to propel the matter along the whole length of the arch. Instead, the matter fell back along the loop, and the process was repeated periodically. Because of this periodic reorganization, it was conjectured that energy sufficient to trigger a flare could not be built up.

1.3.4.2 Observations of Velocity and Magnetic Shears in Flaring Regions

Evidence of sustained magnetic and velocity shears in an active region, reported by Athay *et al.* (1984), was discussed at the SMM Workshop by H. P. Jones. The authors com-

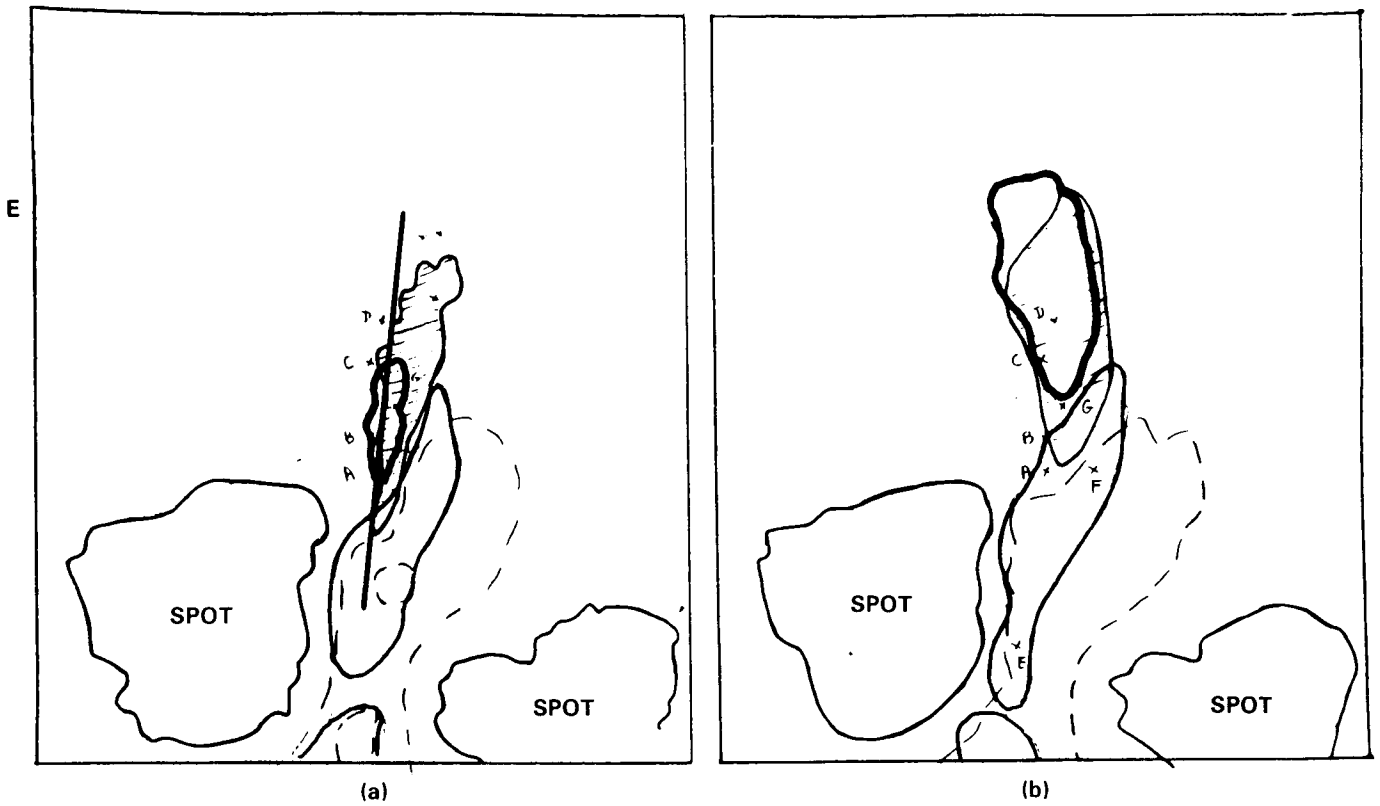

Figure 1.3.13 Evolution of Hα intensity and velocity during the surge event at 12:32 UT on September 1, 1980. The two spots indicated are the N-polarity spots shown in Figure 1.3.12 that compressed the smaller, S-polarity spots, causing recurrent surging on this date. The shaded regions indicate areas of diminished Hα intensity whereas the dashed curve outlines areas of enhanced intensity. The solid contours outline Doppler-shifted areas with the darker (lighter) contour representing upward (downward) velocities. (a) 12:33:20 UT. (b) 12:36:20 UT. The field-of-view in both frames is 1′ × 1′. The projection of the surge axis on the solar surface is depicted in (a) by the solid line.

pared UVSP Dopplergrams and spectroheliograms in C IV, Si IV, and other UV lines for Hale region 16918 (Boulder region 2517) with ground-based magnetograms, Dopplergrams, and spectroheliograms taken at Kitt Peak, and with Hα filtergrams taken at Big Bear Solar Observatory. The active region was in a complex which passed across the solar disk in the latter half of June 1980. The region was characterized by an unusually long magnetic neutral line that ran more or less eastward from its western extremity for some 300″, and then curved rather sharply in a southeastward direction for about 600″. A set of six Kitt Peak photospheric magnetograms is shown in Figure 1.3.14; the two segments of the neutral line are quite evident on the magnetogram for June 19. A complex, time-varying system of Hα filaments paralleled the magnetic neutral line; several filaments with footpoints anchored in regions of opposite polarity were spaced at wide intervals along the neutral line. Along the east-west segment, the filaments tended to be long, gently curved, and frequently quite broad in their north-south dimension. Filaments along the second segment of the neutral line were shorter, more curved and of shorter lifetime than those in the east-west segment.

UVSP Dopplergrams were made simultaneously in Si II and C IV several times per day during the period of observations of this region. Dopplergrams in C II were made during one orbit on June 17, and a series of Dopplergrams were made in Fe XII on June 17,18 and 19. Figure 1.3.15 exhibits examples of the Dopplergrams made in these four ions. Ground-based Dopplergrams were made in the Fe I (8688 A) and Ca II (8542 A) lines on June 18, 19 and 20. The authors found similar velocity patterns in C IV, C II and Ca II, although the areal extent of the observed pattern decreased in the order given. Examination of the magnetic and velocity data showed an inversion line in the line-of-sight velocity fields in the transition-region and chromosphere which conformed to the extended, stable, magnetic inversion line. The lateral gradients in both magnetic and velocity fields across this "neutral" line were strong and sharp; this structure maintained its general character for well over a week. From the C IV Dopplergrams, they found velocity differ-

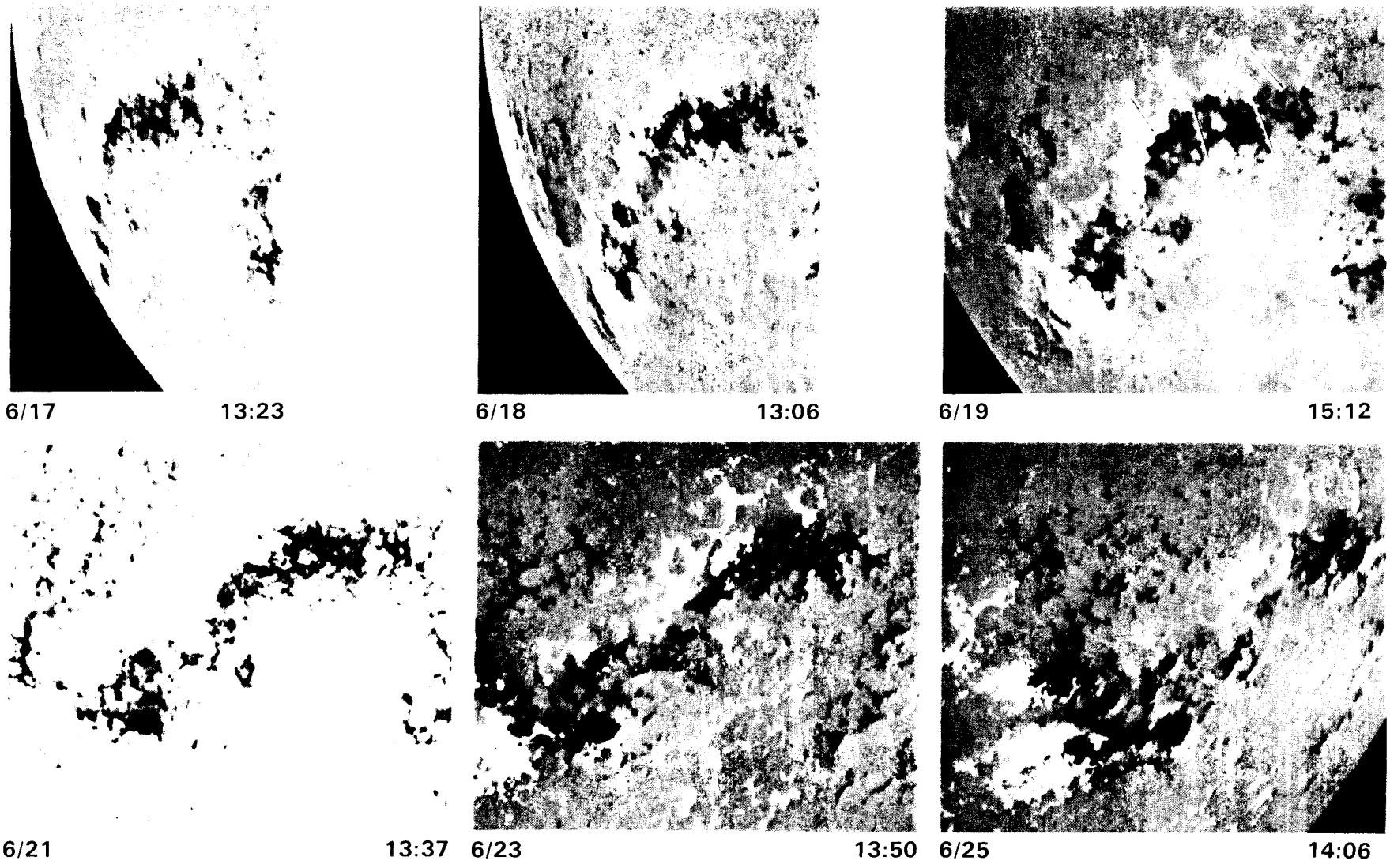

Figure 1.3.14 Magnetic evolution of AR 2517 for the period June 17-24, 1980. The individual frames are portions of six full-disk photospheric magnetograms taken at Kitt Peak. White and dark areas denote positive and negative line-of-sight magnetic fields, respectively.

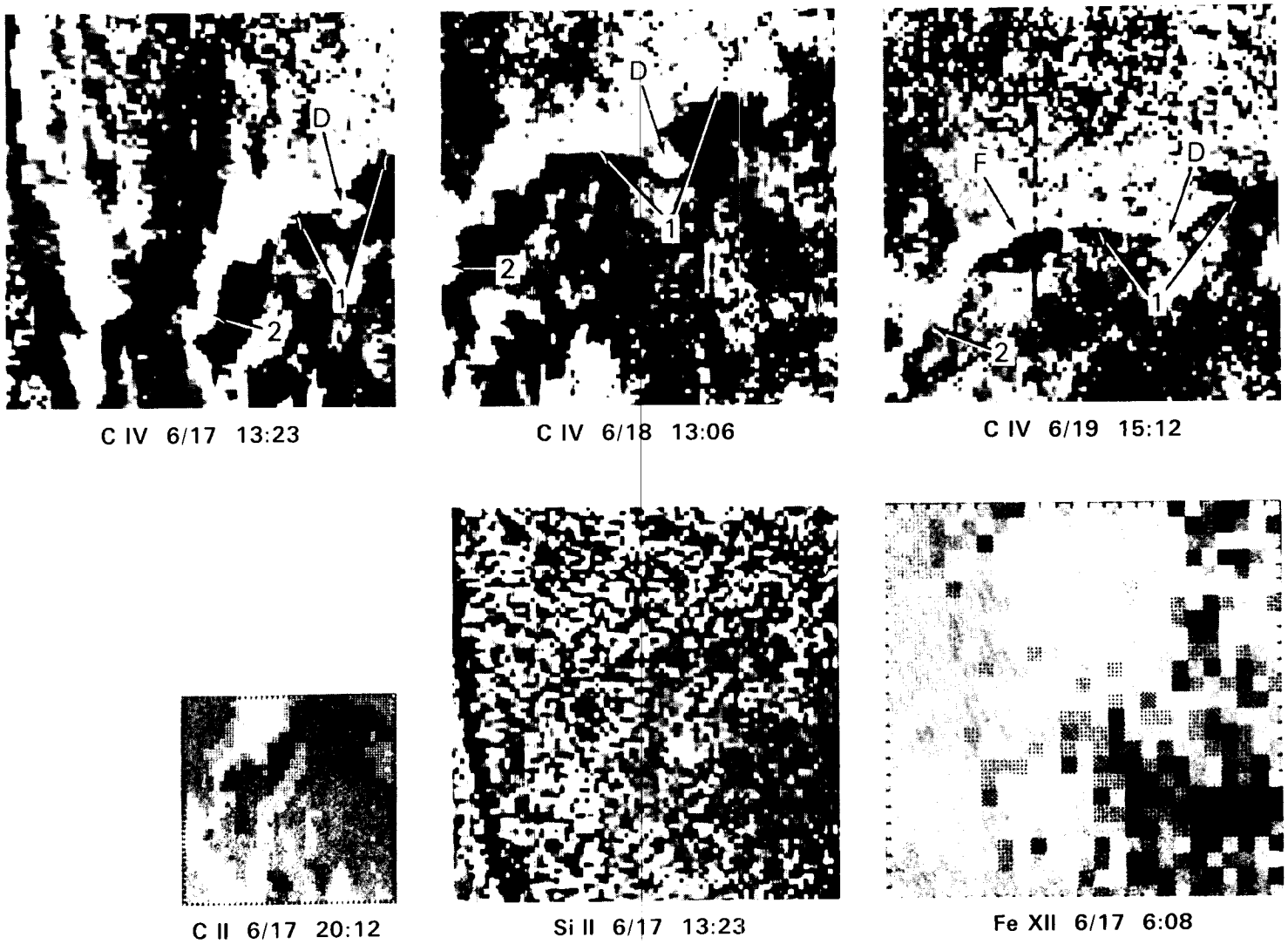

Figure 1.3.15 UV Dopplergrams of AR 2517 for the period June 17–19, 1980. All frames are to the same scale with fields-of-view of 4′ × 4′ for the larger frames. Red shifts are shown in white. The C IV and Si II Dopplergrams are corrected for solar rotation to mimic the observing times of the corresponding magnetograms in Figure 1.3.14. Note the absence of any clear pattern in the Doppler signals for the Si II and Fe XII lines.

ences between adjacent red and blue shifted bands either side of the velocity inversion line that frequently exceeded 20 km s^{-1}. The average velocity gradient across the inversion line was approximately 2 km s^{-1} $arcsec^{-1}$, and this steep gradient often persisted for distances of 9″. In the chromospheric Ca II data, these values were reduced: the maximum velocity gradient was 0.5 km s^{-1} $arcsec^{-1}$, and the maximum velocity difference across the inversion line was about 1.8 km s^{-1}. The authors inferred that there was a strong horizontal component of the velocity field since the flow pattern weakened as the region approached central meridian and changed sense after meridian passage. This effect is illustrated by the three C IV dopplergrams for June 17, 18, and 19 in Figure 1.3.15. The authors identified the orientation of the fluid flow in the region with the orientation of the magnetic field, assuming that the fluid flow follows the magnetic field.

The resultant picture of the magnetic field near the neutral line was one of extreme shear at the level of the transition region where C IV is formed, diminishing to greatly reduced shear at the photosphere where the magnetic field was observed. Moreover, the simplest velocity pattern consistent with the data was that of material flow diverging from the tops of low-lying, sheared loops that were closed over the neutral line. The data did not provide obvious clues regarding the supply of material to these loops, but the authors suggested that the sheared magnetic and velocity configuration might be sustained by an underlying, large-scale circulation pattern such as the slow convergence of two giant cells of opposing magnetic polarity.

Numerous small flares and emerging flux regions were reported around the neutral line by Martin *et al.* (1983), and the observed transition-region line intensities showed continual brightenings. However, the segments of the magnetic neutral line that showed the most evidence of shear produced very little flare activity; the majority of the activity was mainly associated with emerging flux regions. Evidently, this configuration, with strong magnetic shear in the transition region diminishing to reduced shear in the photosphere, is either rather stable or does not contain an abundance of free energy.

1.3.4.3 Vortical Velocities Near Flaring Sites

The Solar Department at the Paris-Meudon Observatory carries out simultaneous observations with ≈2″ spatial resolution in Hα and photospheric spectral lines to study chromospheric structures, line-of-sight magnetic and velocity fields, and flare locations. These studies led to the recognition of large-scale (15-20″) structures in both the magnetic and velocity fields: evolving magnetic structures (e.g., Martres *et al.*, 1968) and star-shaped and vortical velocity patterns (Martres *et al.*, 1973). The appearance of combinations of these patterns has been related to magnetic evolution and solar flares (Martres *et al.*, 1974, 1977).

During the workshop series, the Preflare Group tried to identify flare events for which there were observations of vortical motions and transverse magnetic fields. Only one active region was found, AR 2490, which was discussed previously to illustrate the correspondence between the occurrence of vortex motions and flares on June 7 and 8, 1980. Figure 1.3.16a shows the line-of-sight field as measured by the MSFC vector magnetograph on the 7th at 17:40 UT; an area of parasitic polarity is indicated by the arrow. The corresponding transverse magnetic field is seen in Figure 1.3.16b; the area of parasitic (opposite) polarity has been superposed on this image to aid in orientation. The field direction appears sheared along the eastern and western sections of the magnetic neutral line separating the parasitic polarity from the field of the large sunspot. However, it is difficult to interpret these data because the area is so small. The location and sense of rotation of the vortex pattern observed by the Meudon group at 8:49 UT on the 7th is indicated on a plot of the sunspot's intensity in Figure 1.3.16c. The observation of the vortex motion took place during a flare (8:45 - 8:52 UT) in the vicinity of the vortex cell; later observations at 12:09 UT on the 7th showed no signature of a vortex cell in this area. It is interesting to note that this vortical pattern occurs in an area of large horizontal gradients of the transverse field: just to the south of the parasitic polarity in Figure 1.3.16b the transverse field is very weak, whereas to the west of the neutral line the transverse component is larger than in any other area of the field-of-view. Since the vector field was observed almost 9 hours after the detection of such correlations. Clearly, future coordinated observations are needed to study these interesting phenomena.

A preliminary simulation of the short-term evolution of vortex cells by Rayrole and Berton was outlined at the workshop by Martres. The study involved the observation and analysis of magnetic and velocity data for AR 2438 on May 10, 1980. Observations of the velocity field in this region are shown in the top row of Figure 1.3.17; they show the evolution of the velocity during the interval 13:20 to 14:00 UT.

To interpret these observed patterns, Rayrole and Berton performed numerical simulations that combined different vortical flows with typical Evershed motions. The parameters for the simulations were (1) the profiles of the vertical and horizontal components of velocity, V_Z (r) and V_H (r), where r is the distance from the origin of the coordinate system chosen for the structure, (2) the profile of ϕ (r) = $\tan^{-1}$ (V_{HT}/V_{HR}), where V_{HT} and V_{HR} are the tangential and radial components of V_H (r), and (3) the maximum values V_Z, V_H and ϕ of the respective velocity profiles. The assumed horizontal velocity patterns are shown along the bottom row of Figure 1.3.17. Initially, the velocity pattern was a pure Evershed flow. This was followed by the development of a central vortex cell and then an outer vortex cell. The middle row of Figure 1.3.17 depicts the resulting "Doppler-

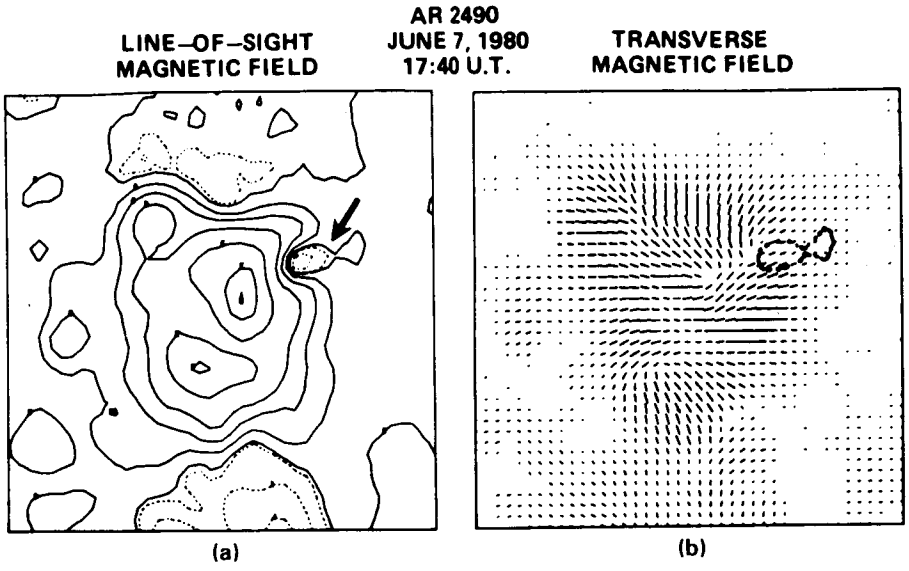

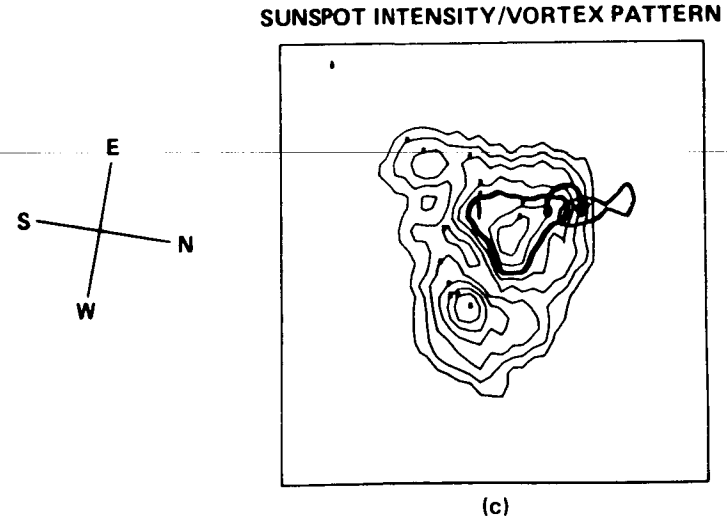

Figure 1.3.16 Vector magnetic field in the area of a vortical velocity cell. (a) The line-of-sight magnetic field observed in AR 2490 on June 7, 1980 at 17:40 UT. Positive (negative) fields are outlined by solid (dashed) curves. The arrow points to the region of parasitic polarity where a vortical velocity cell was observed. (b) The observed transverse magnetic field. The line segments represent the strength (length of segment) and direction (orientation of segment) of the field. The region of parasitic polarity has been superposed to aid in orientation. (c) The observed sunspot and vortex cell. Contours represent levels of intensity of the sunspot. The heaviest contour shows the umbral boundary. Again, the region of parasitic polarity has been superposed on this panel. The arrow indicates the location and sense of circulation of the vortex cell that was observed in this region at 8:49 UT. All fields-of-view are 1.67′ × 1.67′.

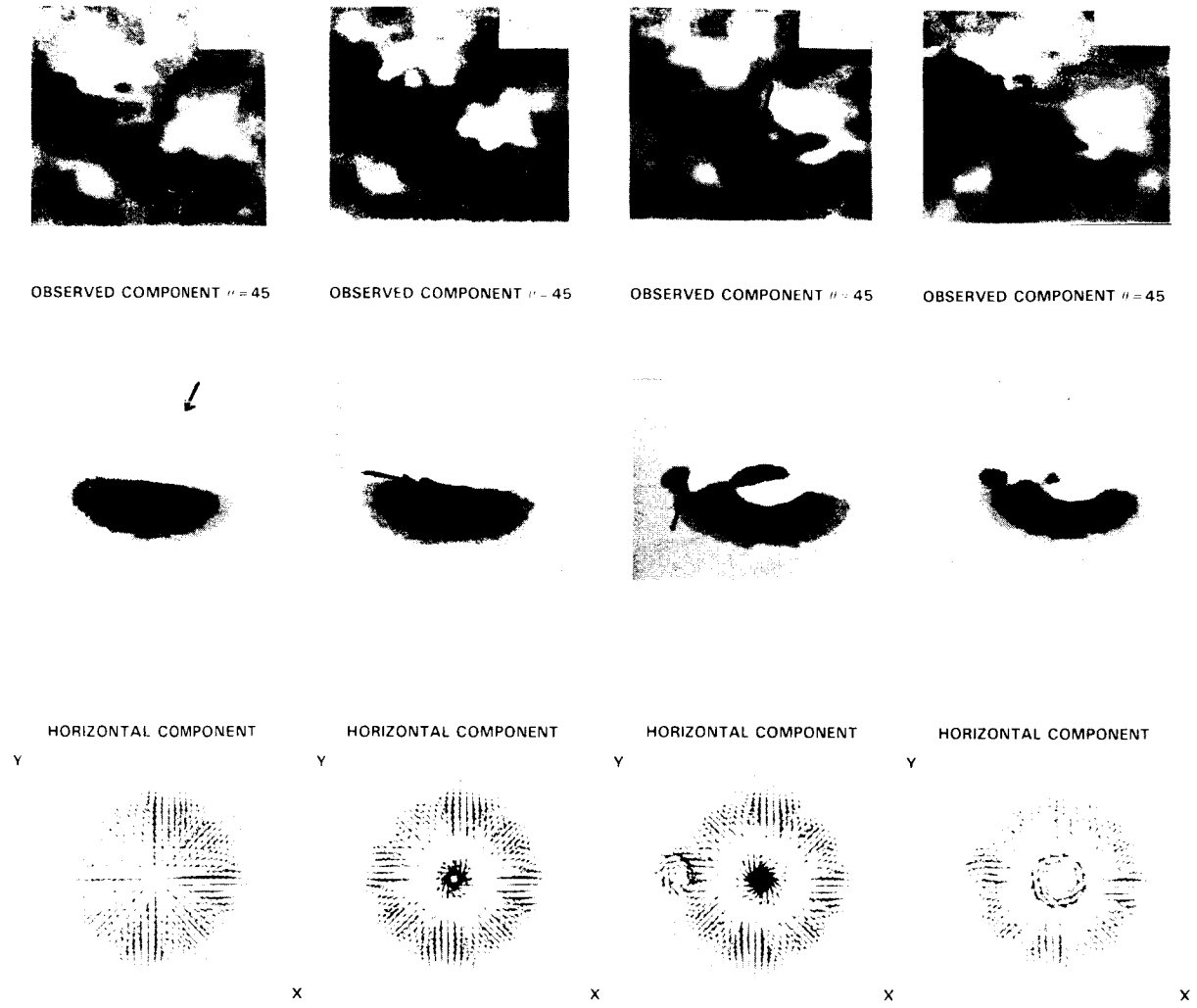

Figure 1.3.17 Comparison between observed velocity patterns in AR 2438 and numerical simulation. Top row: Dopplergrams observed on May 10, 1980, during the period 13:20 to 14:00 UT. Blueshifted (redshifted) velocities are represented by white (dark) shadings. The arrows point to features that are modeled in the numerical simulation. Middle row: "Dopplergrams" generated by numerical simulation. The shadings are similar to those shown in the observed Dopplergrams. Bottom row: the velocity patterns assumed in the numerical simulations. The velocity parameters used in the simulations for each panel are the following: 13:20 UT a pure Evershed flow with a small torsion ($V_Z = \phi$, $V_H = 1500$ m s^{-1}, $\phi = 10°$); 13:30 UT the same Evershed flow but with a central vortex cell with $V_Z' = \phi$, $V_H' = 1800$ m s^{-1} and $\phi' = 20°$; 13:45 UT: the Evershed flow (unchanged), the central vortex but now with a reversed horizontal component ($V_Z' = \phi$, $V_H' = -2000$ m s^{-1}, $\phi' = -20°$), and an outer vortex cell with components $V_Z'' = -400$ m s^{-1} (downward), $V_H' = 1800$ m s^{-1} and $\phi'' = 100°$; 1400 UT: the same Evershed flow, the central vortex with $V_H' = 2000$ m s^{-1} (reversed from the previous time) and $\phi' = 100°$, and now with a strong upward component $V_Z' = 1500$ m s^{-1}, and the outer vortex with a decreased horizontal component, $V_H'' = 400$ m s^{-1}, the same torsion ($\phi'' = 100°$), and an increased downward flow ($V_Z'' = 1600$ m s^{-1}). Note the appearance of the "horseshoe-shaped" structure in the Dopplergram at the site of the central vortex in the simulation for 14:00 UT. This is a result of the nearly equal horizontal and vertical velocities: $V_Z'/V_H' \approx 1$.

grams" that would be observed as a result of these configurations of velocity. Comparisons of the middle and upper panels of Figure 1.3.17 show that the numerical simulations show similarities with parts of the observed Dopplergrams.

The appearance prior to flares of these intriguing vortex patterns in the vicinity of the flaring areas raises the question of their relationship to the sites of maximum shear observed in the magnetic field at flare onset. Certainly, observations imply that the magnetic shear is a fairly persistent feature throughout a flare epoch, whereas the vortical flows only appear 10-60 min before the flare. Thus, the available observations do not support a scenario wherein the vortex motions produce the increased shear at the flare sites. However, more coordinated observations of the vortical velocity patterns and the transverse magnetic field should be carried out to investigate this further. Perhaps the magnetic shear is caused by vortex flows of smaller magnitude than can be detected at the present time. To resolve weak shear motions, it is necessary to average a number of Dopplergrams to overcome the effects of atmospheric seeing, short-lived vertical motions and the 5 min oscillations.

1.3.5 Emerging Flux

The long-established association (Giovanelli, 1939) between flares and changing, especially growing, magnetic fields has been confirmed and extended by many subsequent analyses (Martres *et al.*, 1968, Smith and Howard 1968, Rust 1972). Observations of flare-associated filament eruptions over growing pores (Rust and Roy 1975, Rust *et al.*, 1975) led to the proposal of a specific mechanism to produce two-ribbon flares: the reconnection of newly emerging flux with an overlying filament (Canfield *et al.*, 1974). This mechanism is central to the Emerging Flux Model developed by Heyvaerts *et al.* (1977). Now emerging flux figures in several models of the preflare state as either continuously driving a flare or triggering it from a metastable state in which magnetic energy has accumulated.

Although the Emerging Flux Model is rooted in observations, its empirical verification in the form pictured by Heyvaerts *et al.* (1977) is by no means simple. A basic problem lies in the profusion, over a wide spatial range, of magnetic changes. Magnetic flux frequently appears as intensely concentrated bundles in the presence of existing flux. Such changes arise, for example: at the birth of new active regions in the "old" chromospheric network (Bumba and Howard 1965, Born 1974) in already growing active regions at the rate of one or two pairs of bipolar "points" per hour (Schoolman 1973); as "satellite spots" (Rust 1968); as ephemeral regions scattered over the entire solar surface, of which hundreds form and disappear per day (Harvey and Martin 1973); and as "complexes of activity" (Gaizauskas *et al.*, 1983). With enough spatial resolution and magnetic sensitivity, one should not be surprised to find, during high solar activity, some changing magnetic fields conveniently close to any flare.

How then to discriminate between those changes in magnetic flux whose proximity to a flare is coincidental and those which could conceivably initiate reconnection (e.g., Priest, 1984a, 1984b) or some other process of destabilization (e.g., Hood and Priest, 1980; Kuperus and van Tend, 1981)? The evolution of the flux and the thermal history of its environs must be followed continuously from its first appearance in order to test its relevance to any associated flare. Ideally, we need to measure: the rate, duration, magnetic field intensity and total flux of the new magnetic fields; the magnetic topologies of the emerging flux and of its surroundings; the relative orientation of new and pre-existing magnetic fields; the relative motions of interacting magnetic field patterns, including internal shears; and the changing radiative output with time from photospheric to coronal heights above the increasing magnetic flux. The opportunities to make such measurements existed during the coordinated observations of the Solar Maximum Year. The practical difficulties are such, however, that these ideals were not fulfilled for a single flare.

Evidence that at least some flares are produced by reconnecting "new" and "old" magnetic flux is confused because important details are obscured or still beyond our grasp. Basic concepts about preflare process thus remain unsettled. We shall discuss specific flares associated with the appearance of magnetic flux, which were discussed during the SMM Workshop. But first we examine the background of basic empirical facts concerning flux emergence; for more details, the reader is referred to reviews by Zwaan (1978, 1981).

1.3.5.1 Signatures of Emerging Flux

(i) Chromospheric. The emerging flux model presupposes that magnetic flux rises vertically from beneath the photosphere as bundles of flux tubes in the shape of loops. This fundamental concept is firmly rooted in the customary pattern of growth of bipolar concentrations of magnetic flux ranging in size from ephemeral regions to sunspot groups (Zwaan 1978). While an active region is in its phase of rapid growth, it is referred to as an Emerging Flux Region (EFR, after Zirin, 1970, 1972). The EFR usually has a characteristic signature in the chromosphere which is an important diagnostic for locating new magnetic flux and for tracing its evolution, the Arch Filament System (AFS, after Bruzek, 1967). An AFS consists of a succession of parallel, low-lying arches which bridge the dividing line between opposite polarities in a newly forming group of sunspots. These arches have a distinctive velocity pattern: an ascending motion at the top (< 10 km s^{-1}) and stronger flows (≈ 50 km s^{-1}) down each branch to the footpoints (Bruzek 1969, Roberts 1970). The arches are embedded in conspicuously bright and amorphous Hα plage which extends along the entire length of the arches while an EFR is evolving with its greatest vigour.

An EFR will sometimes be resolved into tightly-packed clusters of Ellerman bombs ("moustaches") and their attendant surges when the region is viewed at Hα ±1.0 Å (Bruzek 1972). The pronounced flow patterns, the intense (almost subflare-bright) plage, and the underlying Ellerman bombs, plainly distinguish AFS from other low-lying arches, the Field Transition Arches (Zirin, 1974), which sometimes replace an AFS in its later evolution. The AFS lasts for 3-4 days in the case of an EFR which matures into bipolar spots with penumbrae and with typical lifetimes of 2-3 weeks (for details, see Weart, 1970; Frazier, 1972; Zirin, 1974; Zwaan, 1978). For ephemeral regions and short-lived active regions, the AFS may last from a few hours to about a day.

Observations at high spatial and temporal resolution of the pre-AFS phase are still so sparse that few key properties of this critical phase of the growth of active regions can be stated with assurance. For example, Martin (1983) claims the existence of an earlier state of development of an active region: a succession of very small flares and associated surges seen one or more hours before the appearance of an AFS. The relation has yet to be determined between the onset of this dynamic stage and the first appearance of a new bipolar field at the photosphere. There is general agreement however that the first chromospheric response to an emerging bipole is the conspicuous brightening of chromospheric faculae observed in Hα and Ca II K (Bumba and Howard 1965, Born 1974, Glackin 1975, Kawaguchi and Kitai 1976). But for an estimation of the delay between the detection of a bipole at the photosphere and the chromospheric response, we must appeal to studies of the more numerous ephemeral regions which are believed to be indistinguishable from active regions at their onsets. It takes about 15 min to be sure that a new ephemeral region bipole has formed, depending upon spatial resolution and sensitivity of the magnetograph; the Hα brightening is detectable within another 30 min (Harvey and Martin 1973). The first arch of an AFS then appears from an hour (Glackin 1975) to about 1.5 hour later (Kawaguchi and Kitai 1976).

Once an AFS forms, the lifetime of individual flat arches is about 20 min; they fade without individually changing length and are continually renewed as long as the AFS is active (Bruzek 1967). On the assumption that every Hα arch traces a magnetic loop, Born (1974) estimated that each brings $\approx 10^{19}$ Mx to the surface. Few ephemeral regions form an AFS; there is some suggestion that a threshold of $\approx 1.5 \times 10^{20}$ Mx for the total flux of an ephemeral region must be exceeded in order to support an AFS (Harvey and Martin 1973).

(ii) Coronal. The morphological description given in the review by Sheeley (1981) of the multithermal coronal plasma associated with emerging flux is based on XUV spectroheliograms obtained with the NRL Skylab/ATM slitless spectrograph. No examples have yet been published of simultaneous chromospheric and coronal observations at high temporal resolution sustained over the birth of an EFR. Most of the following summary, taken from Sheeley (1981; 1980), pertains to the coronal geometries of partially evolved EFR's.

The low temperature EFR plasma (at the 0.5×10^6 K temperature of Ne VII) is confined to the footpoints and legs of magnetic field lines; it rarely forms complete loops. The most striking Ne VII features are long spikes which diverge from the outer ends of an EFR, i.e. from the outer edges of the spots which are normally growing at each end of a bipolar EFR. The spiky structures project 10^4-10^5 km from their footpoints; each lives on the order of 30 min. The high temperature plasma (at the 2.0×10^6 K temperature of Fe XV), on the other hand, is confined to relatively diffuse loops or systems of unresolved loops which join opposite poles within the same EFR or between adjacent active regions, presumably along closed magnetic field lines. Unlike the low-temperature features, the high-temperature loops fade out toward the footpoints. Individual high-temperature structures evolve on a time scale of roughly 6 hr while their collective patterns endure for several days or more.

Sheeley and Golub (1979) were able to establish variability on the scale of $\approx$ 6 min in the multiple, small, elongated, high-temperature (Fe XV) structures in both the active region and a coronal "bright point" (possibly associated with an ephemeral region). Their observations suggest that the life history of a single "bright point" consists of continuous sequence of miniature loops which evolve rapidly and independently of each other.

Coordinated observations of ephemeral regions and coronal bright points were performed briefly during the Solar Maximum Mission (Tang *et al.*, 1983). These limited data show that more ephemeral regions are found at the photosphere than are their counterparts at higher levels in the atmosphere. There is no indication that UV bright points (observed in the λ1548 Å line of CIV, characteristic of the transition zone) are enhanced before their associated ephemeral regions are born in the photosphere. Partial UV light curves are available for only two bright points which can be identified with specific ephemeral regions. Brightness of these points maximizes 1/2 and 1 hr after their corresponding ephemeral regions are detected; the brightness drops drastically in the final hour of these two ephemeral regions. (These times are strongly influenced by the sensitivity and spatial resolution of the magnetograph used for their estimation).

At the time of this Workshop, no account existed of the evolution from birth of the spatially-resolved microwave emission from ephemeral regions or EFRs.

(iii) Photospheric. The onset of flux emergence is defined with respect to the photospheric level – specifically by the first detection (e.g., by a magnetograph) of elements paired as a bipolar ephemeral region or a new EFR. Discussion of this aspect of emerging flux has been deferred in order to emphasize the following point: the photospheric feature so

commonly cited in the literature on solar flares, the growing pore, is preceded by other well-defined phenomena in both the photosphere and chromosphere.

Thus Bray and Loughhead (1964) found anomalous alignments and darkenings of intergranular lanes which preceded the appearance of a pore by 3 hr. Strong downdrafts, amounting to 1-2 km s^{-1} or more as measured with photospheric lines (Kawaguchi and Kitai 1976, Bumba 1967, Brants *et al.*, 1981) occur near protopores. The downdrafts are localized in small patches ($\approx 2''$) beside, not inside, a protopore (Zwaan *et al.*, 1984). The downflow lasts for at least an hour and stops after the initial detection of the associated photospheric dipole (Harvey and Martin 1973), or after the appearance of the first arches in an AFS (Born 1974).

An existing pore in an EFR grows by adding new flux at the edge facing the centre of the growing active region (Brants 1983). This behaviour is consistent with the later developments in an active region (Zirin 1974): sunspots invariably form at the outer ends of an active region while new flux is added near the middle. The leading and trailing umbrae grow by coalescence of pores of the same polarity (Vrabec 1974, McIntosh 1981). A major region will attain its maximum flux of $\approx 3 \times 10^{22}$ Mx in several days. A new group of spots spreads apart in longitude at a typical rate of 0.1 km s^{-1} which can be sustained for 5-6 days (Kiepenheuer 1953). At birth, the velocity of separation within an EFR can range from 1 to 2 km s^{-1}; some hours later it drops to 0.5 km s^{-1} or less (Born 1974).

In the simpler circumstances of the more abundant ephemeral regions a conspicuous spreading, at 5 km s^{-1}, is evident in the first minutes after the bipolar pair of magnetic elements are detected (Harvey and Martin 1973, Martin 1984). In about 30 min, the expansion rate of an ephemeral region drops by an order of magnitude and remains roughly steady for typically 6 hr (Harvey and Martin 1973).

In summary, the emergence of new magnetic flux is marked in the photosphere by rapidly spreading bipolar fragments, in the chromosphere by conspicuous brightening of chromospheric faculae followed by the formulation of an AFS with distinctive strong downflow at its roots. Pores appear several hours later.

We do not yet have the observations to relate fine-scale structures in the corona with their individual counterparts in the lower atmosphere during these initial few hours. We specifically exclude, as evidence for emerging flux at coronal heights, rapidly expanding structures such as: coronal transients; coronal loops or arches seen in the λ 5303 Å line; filaments and other mass ejected from a polarity inversion line. Phenomena such as these may rise from other causes than emerging flux, such as for example, reconnection.

1.3.5.2 Flare-Associated Emerging Flux

The association between flares and EFR is strong. But the numerous flares which erupt within an isolated growing region while it is still in the AFS stage are minor ones (Bruzek 1967, Weart and Zirin 1969). More intense flaring is observed when new flux appears within an existing active region, especially if the emergence places following polarity ahead of normally preceding polarity (Zirin 1970, Vorpahl 1973). The importance of interactions between adjacent flux patterns prevails as well as the scale of ephemeral regions. Miniature flare-like events in Hα occur when a spreading bipolar ephemeral region interacts with neighbouring elements in the network (Marsh 1978).

For the larger, more interesting flares, we therefore look at the magnetic changes which can be thought of as flux emerging in a well-developed active region. These can be placed in two broad categories: changes associated with new flux bearing the AFS trademark or changes within already developed patterns of flux without AFS. We consider as well the influence of observed magnetic changes in an active region on the way a filament erupts preceding a flare.

(i) Development of Magnetic Complexity by Emerging Flux. In dealing with the first category of changes, we note that active regions do not form at random. They show a remarkable tendency to cluster in space and time (Gaizauskas *et al.*, 1983) as complexes* of active regions which last for many solar rotations. Liggett and Zirin (1984) measured a rate of flux emergence 27 times higher within active regions than in quiet background areas at the same latitudes. If the packing density of new regions within a complex becomes high enough, we can expect greater magnetic complexity also, and therefore enhanced flare productivity (Giovanelli 1939, Smith and Howard 1968, Bell and Glazer 1959). This is not a common occurrence. Present knowledge indicates that complexity can develop in several ways when two or more bipolar EFR overlap: either beginning with their simultaneous appearance as AFS (Weart 1970), or from the later intrusion of an EFR into a mature, closely-spaced active region (Zirin and Tanaka 1973, Tang 1983, Zirin 1983), or even from the expansion and interpenetration of adjacent bipolar active regions at the same latitude (Tang 1983). The time in the evolution of the region and speed of superposition are probably key factors.

For the SMM Workshop, Gaizauskas and McIntosh (1984) investigated how the rejuvenation of magnetic flux in complexes of activity affects flare productivity. They compared two sets of homogeneous data for the same 27 solar rotations between 1977 and 1979; the set of flares classed M_1 or stronger from among all 1900 X-ray flares recorded in that period by the SMS-GOES satellites; and the set of synoptic maps of the photospheric magnetic field produced by the Kitt Peak National Observatory (Harvey *et al.*, 1980). The subset of 384 flares so defined is not distributed randomly among the 934 active regions enumerated during the same interval. One-half of the flare subset is accounted for

*"Complex" used in this sense and without a modifier refers exclusively to spatial and not magnetic complexity.

by only 12 regions, the other half by another 65; a tenth of the subset erupted in one hyperactive region, McMath 15403 (CMP on 15 July 1978).

The 77 regions with strong flares, clustered in 37 complexes of activity, are marked according to the class of their strongest flares on the chronological arrays shown in Figure 1.3.18 of active-belt strips from the KPNO synotic maps (cf. Figures 2 to 4, Gaizauskas *et al.*, 1983). For half of the complexes, flaring continues above the M1 threshold for 2 or more rotations. In extreme cases, powerful flares do occur on the fifth (in an X-class region) or even on the ninth rotation (for an M-class region). But in at least 7 complexes, flares in the X-category occur without an episode of even M-class flares during the preceding rotation. The most conspicuous example of an immediate output of very intense flares in just one rotation is McMath 15403. Its behaviour is compared in Figure 1.3.19 with another flare-rich complex, the so-called "great complex" (Gaizauskas *et al.*, 1983).

For the great complex, Figure 1.3.19a, the magnetic flux jumps suddenly from a low initial level to a high level which remains roughly steady over 6 rotations before it subsides quickly. But the incidence of strong flares in this same complex is more erratic as indicated by the X-ray Flare Index (XFI, hatched bars). The XFI is both high and low during the strong outbreak of flux sustained for 6 rotations. When the XFI is high, the great complex consists of extended clusters of large spots with many EFR and strong shears; later, when the XFI is low, the great complex contains only one large spot, some EFR and considerable flux distributed throughout the photospheric network. In contrast, hyperactive region McMath 15403 reaches a relatively high flux level and very high XFI in just one rotation (Figure 1.3.19b). During its visible passage, it is a compact and formidably complicated δ-configuration.

Another example of rapid, highly localized development of magnetic complexity occurs during the evolution of the complex activity containing Hale Regions 16862, -3, -4 from 1980 (Gaizauskas 1983) to June 1980 (Martin *et al.*, 1983). Only one new region formed during the first passage of this complex: a very compact δ-configuration which formed in less than a day and produced the only energetic flares for that entire disk passage. On its second passage, 17 new bipolar regions were identified within the evolved complex in an 8-day interval. The great majority of flares, mostly subflares, then erupted within EFR or on their boundaries (Martin *et al.*, 1983), or in locations where new flux appeared adjacent to recently evolved flux from the same rotation (Schmahl 1983).

The build-up of severe complexity is thus more likely to involve new patterns of flux appearing within a few days rather than patterns differing in age by as much as one rotation of the Sun. This finding is consistent with the rapid disappearance, *in situ*, of large quantities of magnetic flux and its rapid replacement by new, differently arranged flux in a still-active complex (Gaizauskas *et al.*, 1983). The months-long survival of complexes of activity is not in itself sufficient to buildup magnetic complexity as supposed by Bumba and Obridko (1969).

Currents flowing in the strongly sheared and twisted magnetic fields in magnetically complex regions are presumed to buildup a reservoir of "free energy" which is then released in flares (Nakagawa and Raadu 1972). These concepts encounter difficulty, however, with the phenomenon of flare homology. Experience during the SMY indicates that homology is not at all rare (Woodgate *et al.*, 1983) and must be included among the constraints on flare models. If prior storage of energy is a necessary condition, it must be released by the same process in the same spatial domain in order to reproduce the geometries and time profiles of the flare emissions in a chain of homologues. Now, if flares are "released" by a mechanism which operates as a simple safety valve attached to a constantly stressed reservoir, the output energy ought to remain the same for each flare in a homologous chain. On the other hand, if the release mechanism is not continuously operative, the output energy per flare ought to be proportional to the build-up time between activations of the release mechanism.

Neither steadiness nor proportionality of output were evident for the chain of 5 homologous flares observed within 13 hours, 28-29 May 1980 in a compact δ-region (Gaizauskas 1983). The compactness makes it difficult to distinguish with certainty between relative motions of pores (Nagy 1983) and their appearance or disappearance in a few hours, with new flux possibly appearing in nearly the same place. Yet it seems implausible that new flux, if it were to be acting as the flare-release mechanism, would re-emerge in precisely the same location and in the same manner so many times in succession. The variation of output energy per flare, despite the close homology in this instance, suggests that flares could be driven from the source whose energy supply determines the ultimate flare energy. For example, this chain of flares could have arisen from the shearing action produced during the rapid relative motions of adjacent pores in such a way that the deformation of the magnetic field was not uniform with time.

At some point in the growth of a bipolar active region, the emergence of its flux must stop. Other new bipoles may continue to appear nearby as part of a process for sustaining a complex of activity. Their signatures are easily recognized (§1.3.5.1) and correspond, to the best of our knowledge, to flux which emerges from well below the photosphere. But other prominent changes in magnetic flux happen in well-developed active regions without these signatures; they too figure in flares. The origin of these features being uncertain, they are designated here as "appearances" rather than "emergences".

For example, magnetic flux outflow (Vrabec 1974) appears around the edges of some large-spot penumbrae as a rim of reversed polarity moving radially away from the spot

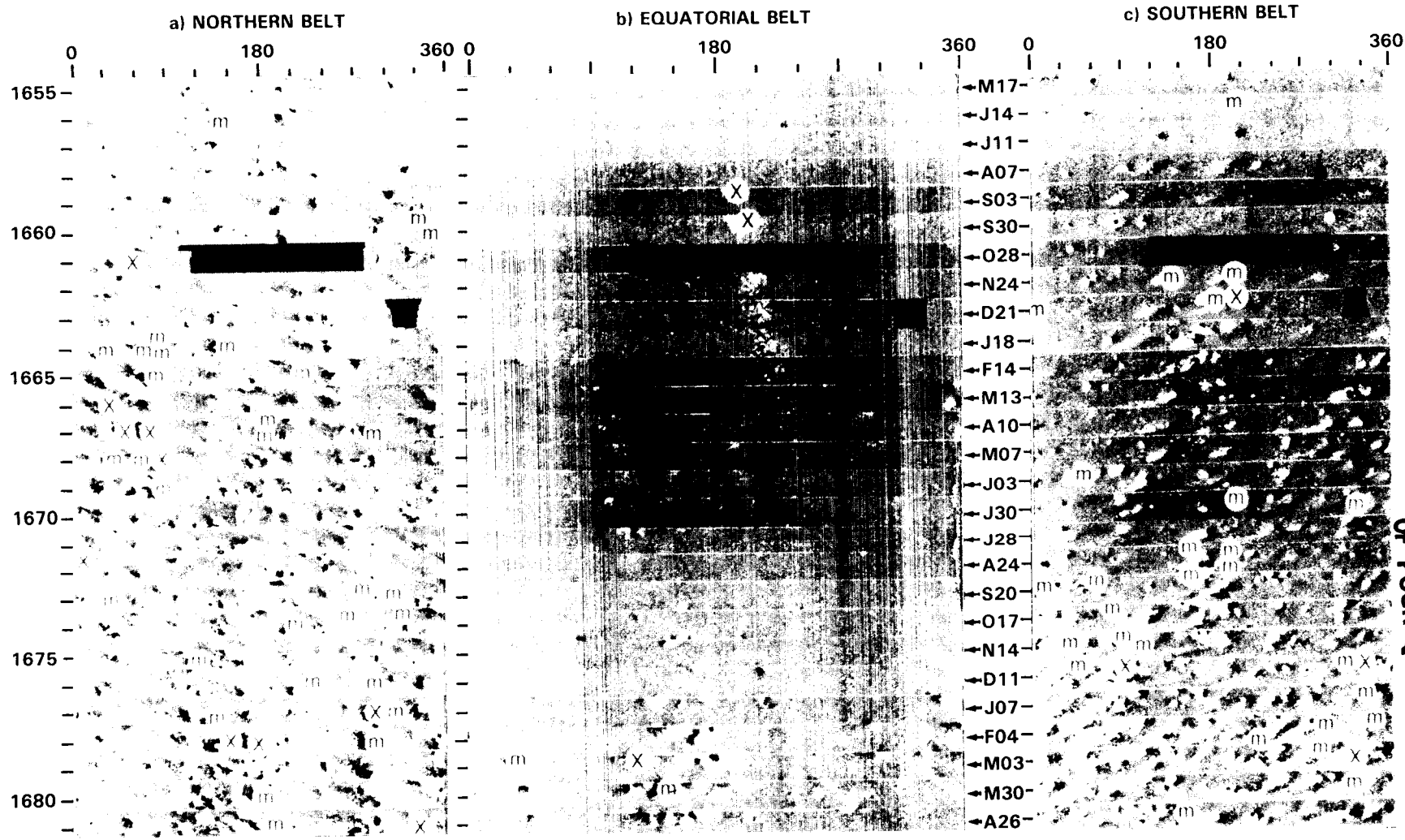

Figure 1.3.18 Chronological arrangement of KPNO synoptic magnetograms of magnetic flux density adapted from Gaizauskas *et al.* (1983). The Carrington rotation number for each strip is shown in the extreme left column. (a) Latitude belt 10°-40° N for each strip of 0-360° in longtitude. (b) Equatorial belt of latitudes, 10°S-10°N for each strip of 0-360° in longitude. (c) Latitude belt 10°-40°S for each strip 0-360° in longitude. The regions in which they occur are designated as "m", "X", or "Z" according as they contain at least one flare classed, respectively, from M_1 to M_9, X_1 to X_9, or X_{10}, in the SESC system.

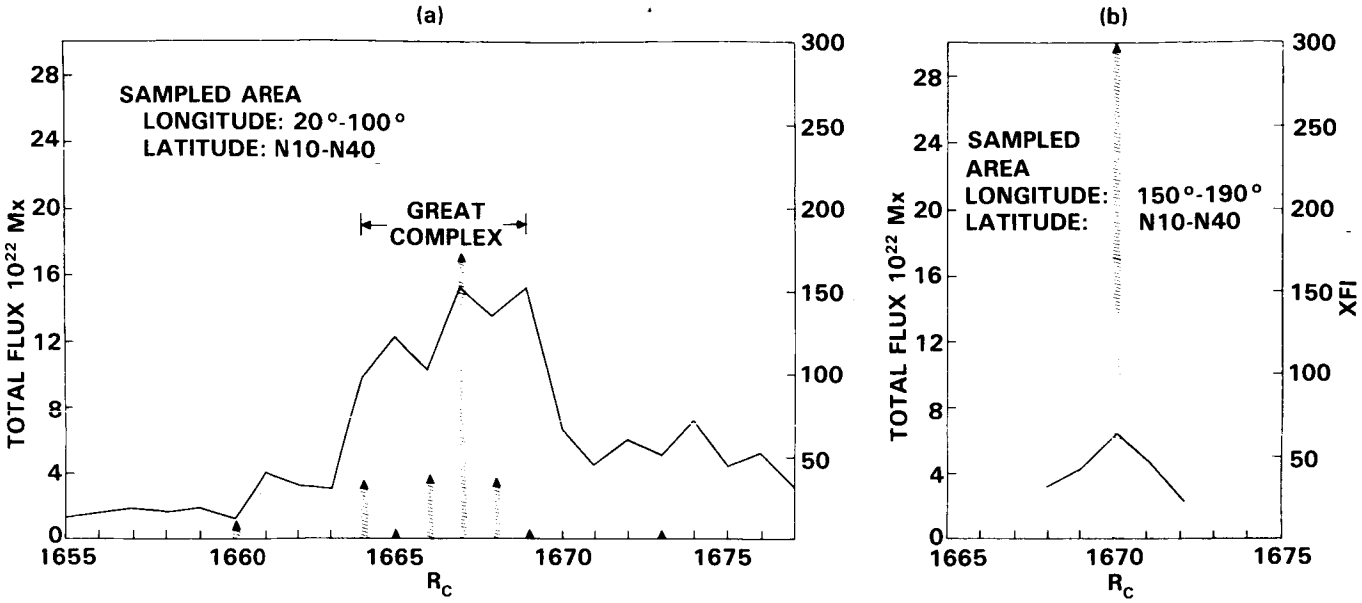

Figure 1.3.19 Episodes of strong X-ray flare activity during the evolution of complexes of activity: (a) in the latitude-longitude limits enclosing the great complex of activity, April-July 1978; (b) in the latitude-longitude limits enclosing the hyperactive McMath Region 15403 (one-half the area of (a)). Abscissa is the Carrington rotation number; left ordinate is the total flux density in the enclosed area; right ordinate is the X-ray Flare Index (XFI) in both panels. XFI = $\Sigma j(M) + 10\Sigma j(X)$ where j(K) is the multiplier used in X-ray class K (K = either M or X). For an X3 flare J(X) = 3 so that its XFI is 10 times greater than for a single M3 flare.

with steady speeds $\approx$ 0.2 km s^{-1} and greater (Sheeley 1969, Harvey and Harvey 1973). It appears without forming AFS and without enhanced Hα emission even though its average flux may be $\approx 10^{19}$ Mx (Harvey and Harvey 1973). Magnetic flux outflow can produce many small surges and even small subflares (Roy and Michalitsianos 1974). Its relationship to other persistent flaring sites on the periphery of sunspots, the so-called "satellite sunspots" (Rust 1968) is uncertain. During observations coordinated with SMM in May 1980, a location of intermittent magnetic flux outflow activity on the rim of the leading spot in Hale 16863 was found to persist for several days as a favoured site for miniature surges and subflares (Gaizauskas 1983). Magnetic flux outflow is believed to be part of a process whereby a sunspot dissolves through fragmentation of its flux tubes (Harvey and Harvey 1973). In that sense, magnetic flux outflow is conceived as a redistribution of already emerged flux, rather than an emergence from a great depth.

Even less understood than magnetic flux outflow is the appearance of pores and small spots without AFS in the middle of mature bipolar active regions. Pores can be found in profusion around the polarityinversion lines underlying the field-transition arches in large, slowly spreading regions like Hale 16863, -4 (Gaizauskas 1983). At the SMM Workshop, Schadee provided examples of transient miniature X-ray events in the lowest energy (3.5-5.5 keV) channel of the HXIS. The low background noise in this instrument allows the detection of very weak X-ray sources. These sources are abundant in field-transition arches and in general along polarity-inversion lines of mature active regions (cf. Gaizauskas 1983, Figure 10). Some sources enact the 2-ribbon flare scenario in miniature, such as the tiny subflares in mature region Hale 16850 which erupted adjacent to the very long filament which separates still-evolving network of opposite polarities (Schadee and Gaizauskas 1984). VLA observations at 6 cm of other bipolar regions show that radio sources over similar areas of transverse magnetic fields are brighter than those associated with sunspots (McConnell and Kundu 1984).

No systematic study has yet been made to explain why a bipolar AFS transforms into a bipolar region with field-transition arches, why coronal emission is enhanced and eruptive along these polarity inversions, or whether the pores appearing at this stage bear any special relation to the field-transition arches. We may speculate that some of the rapid appearances of new photospheric structures in the middle of mature active regions represent a concentration of superficial flux rather than the emergence of deep-rooted flux. Whatever the origin of these new concentrations, it is in just these circumstances of late development in the active regions that the 2-ribbon flares, advanced in support of the emerging flux model, have occurred (Rust and Roy 1975, Rust *et al.*, 1975, Rust and Bridges 1975, Canfield and Fisher 1976, Hoyng *et al.*, 1981, Simon *et al.*, 1984, Moore *et al.*, 1984).

(ii) Filament Activations and Emerging Flux. Strong circumstantial evidence links the appearance of new pores with flares for the events just cited. But an attempt to extract from

them the quantities needed for a rigorous test of the Emerging Flux Model is soon frustrated by the lack of essential pieces of information. Missing most frequently from the examples cited above are the velocity fields associated with emerging flux and the morphologies of fine structures which would yield the relative orientations of new and pre-existing magnetic fields. Breaks in the data at critical periods further amplify the uncertainties. Conclusions drawn from changing patterns of magnetic fields remain inferences based on the premise that rising flux creates the changes.

The small pores of opposite polarity which are believed to figure in the destabilization of a filament as described by Simon *et al.* (1984) approach each other, contrary to the normal spreading action in an EFR. No direct evidence is provided that these pores are linked magnetically to each other or to the filament; their presence and proper motions are suggestive but enigmatic. For the well-studied class 2B flare of 1980 May 21, Hoyng *et al.* (1981) attribute the destabilization of a long filament over an extended polarity-inversion line to the emergence nearby of a bipolar region containing a new pore. Subsequent analysis of magnetograms by Harvey (1983) suggests that the pore formed not by emergence but by the compression of existing flux at the surface. New flux did appear nearby as patches of polarity opposite to their unipolar surroundings and in such a way that the shape of the polarity-inversion line was sharply altered. The net flux at a location directly beneath the activated filament actually decreased. These changes may have destroyed the equilibrium between the filament and its surroundings without recourse to reconnection.

An example of preflare filament eruption without associated emerging flux is the 1980 June 25 class 1B flare at 1552 UT studied by Kundu *et al.* (1985) and discussed at length during the SMM Workshop. The filament was located in the trailing part of AR 2522 (Hale 16931). This region contained two sites of emerging flux which produced several subflares on that same day: on the northern rim of the large leading spot, and in a small magnetically complex region immediately SE of the erupting filament. An adjacent region of comparable size, AR 2530 (Hale 16923) had even more extensive emerging flux in its mid-section. The flare-associated filament was only 40,000 km long; its midpoint passed close to a compact cluster of pores which had no associated chromospheric activity. A close examination of KPNO magnetograms taken hours before and after the flare shows minor, subtle changes in the magnetic flux of photospheric structures adjacent to the filament (Kundu *et al.*, 1985). Nothing observed in 7 hours of rarely interrupted wavelength-sweeping across Hα at high spatial resolution with the photoheliograph at the Ottawa River Solar Observatory can be suspected as adjacent emerging flux which might trigger a filament eruption.

Strong proper motion of the leading sunspot in AR 2530 ($\approx$ 150 m s^{-1}) implies strong shearing near the inter-region boundary which intersects the active filament at its western footpoint (Schmahl 1983). There were no significant proper motions of the spots in which the filament terminated or of the pores near its mid-point. The regions were sufficiently far from the center of the disk that perspective aids the determination of the velocity structure of the filament. Its lateral displacement can be followed with respect to the fixed pattern of photospheric features. Doppler shifts indicated by off-band filtergrams give the sense and an estimate of the line-of-sight velocity. The combined measurements show that the center of the filament began rising slowly ($<$ 1 km s^{-1}) about 3 hours before the flare and accelerated steadily but not uniformly right into the eruptive stage. Matter drained down each end of the filament. About 2 hours pre-flare, the downflow at the eastern footpoint gained a sudden impetus coincident with the activation of a huge boundary filament on the southern side of AR 2522. This larger structure was co-terminal with the flare-associated filament inside the large, trailing sunspot.

At 20 and 10 min preflare, the Hα blue shifts towards the eastern half of the structure increased substantially while at the same time the lateral movement of the filament ceased entirely. This indicates that the suddenly enhanced Hα blue shifts observed during this period had to arise from axial flow rather than an accelerated upheaval. For these two episodes of enhanced flows, filtergrams at Hα $\pm$ 0.6 Å were subtracted in pairs. They reveal that the filament was rapidly untwisting in the fashion described by Rust *et al.* (1975) for an event in which new spots strengthened or first appeared adjacent to a filament during its eruption and a subsequent flare. Yet there were no comparable flux changes in the 1980 June 25 event. Bright Hα kernels and an additional short velocity structure appeared behind (and presumably beneath) the most twisted portion of the rising filament for just several minutes during the last episode of enhanced axial flows. These transient features are co-spatial, in projection, with briefly enhanced blue-shifted C IV emission ($\approx$ 10^5 K plasma) detected by the UVSP onboard SMM. We may speculate that these transients are counterparts of the short-lived velocity feature also recorded by Canfield and Fisher (1976) for another erupting filament.

Emerging flux did not figure as a direct trigger of the flare of 1980 June 25. This is not to deny that flux emerging elsewhere in AR 2522 and AR 2530 may have played an indirect role by modifying the global magnetic structure. Or the growth of instability in the filament may have been initiated by a major disturbance in a magnetically connected structure in the same active region.

The emergence of flux is clearly necessary to set the stage for subsequent flare activity on a major scale. That stage-setting is very important and takes place over many hours or even a few days. Of all the flares studied so far, the 1980 May 21 event comes closest to providing direct evidence that further emergence of a small amount of flux triggers release

of a vast amount of energy stored in a sheared filament. But the details of that particular flux emergence are subtle (Harvey 1983); it is by no means clear how the interaction between the filament and emerging flux should be conceived when the adjacent net photospheric flux decreases during the emergence. The experience with the 1980 June 25 flare, where adjacent emergent flux could not be found, should caution us that the flare triggering process is still elusive.

1.3.5.3 Summary and Recommendations for Studies of Emerging Flux

The vigorous advance of theory (Priest 1984a, 1984b) has brought into sharp focus the observational requirements to test the Emerging Flux Model. From an observational perspective, however, even the conceptual role of emerging flux in the flare process is clouded. Growth of magnetic flux is a necessary pre-condition for flares: small flares are common during the AFS stage of an active region: large flares often have their initial kernels rooted in new, rapidly growing flux. But the vast bulk of magnetic flux appears at the surface without producing flares as strong as a M1 event in X-rays. The published cases of flare-associated filament eruptions lack key facts which are needed either to validate the reconnection inherent in the Emerging Flux Model or to constrain the model in terms of our understanding of flux emergence in the absence of flares. One study of a flare-associated filament eruption on 1980 June 25, observed in detail for many hours at heights in the photosphere, chromosphere, transition zone and corona, rules out local emerging flux as either a driver or a trigger of the activation of that particular flare.

An important new result is the association of Cancelling Magnetic Features with Flares (Martin, 1984). These may have a similar role to emerging flux in triggering flares (Priest, 1985), since what is important is the *interaction* of flux, whether through material vertical or horizontal motions.

A major advance towards clarifying this situation would come from coronal observations aimed specifically at the problem of emerging flux. Jackson and Sheridan (1979) found general increases in activity of Type III radio bursts prior to flares, which imply that energy, originating in the emergence of new flux, is entering the corona on a time scale of many hours. We badly need to supplement the detailed chromospheric and photospheric observations of emerging flux, now available, with simultaneous multi-wavelength coronal observations of comparable spatial resolution ($\approx 1''$) and comparable duration (many hours, even days, preceding the emergence). Target regions of emerging flux need to be followed long enough at all levels of the atmosphere to come to grips with the formation of AFS and field-transition arches, and in contrasting emergences of flux accompanied by their well-established signatures from simple appearances of new flux without those signatures. More than semantics are at stake; our concepts of the magnetic interconnections in the latter situation are woefully inadequate. Finally, we need to clarify the association between ephemeral regions and coronal bright points on an individual basis. In so doing, we should gain insight into the dissipative mechanisms which seem to occur with great frequency on a basic scale, and which might be applicable to ordinary flares.

1.4 CORONAL MANIFESTATIONS OF PREFLARE ACTIVITY

E.J. Schmahl, D.F. Webb, B. Woodgate, P. Waggett, R. Bentley, G. Hurford, A. Schadee, J. Schrijver, R. Harrison and P. Martens

1.4.1 Introduction

Recent observations confirm the view that the initial release of flare energy occurs in the corona, with subsequent emissions arising from the interchange of mass and energy between different levels of the solar atmosphere. Knowledge of coronal preflare conditions is essential to understanding how energy is stored and then released in flares. Observational evidence for storage is, however, difficult to interpret owing to our inability to observe the three dimensional structure of the magnetic field and to the lack of coordinated observations with high resolution in space and in time.

More than sufficient energy to power flares can be stored in local magnetic fields on time-scales of hours. Long-term changes include emerging and evolving magnetic flux regions, satellite sunspots, sunspot motions, and velocity patterns (Martin, 1980; Section 1.3 these proceedings). Although such evolutionary changes are considered necessary for the storage of energy leading to especially large flares, it is very difficult to relate specific long-term changes to particular flares since similar changes occur in their absence.

More rapid changes can occur within minutes or a few hours preceding a flare, and they can be more unambiguously interpreted as flare precursors. Clearly, this distinction is arbitrary, but it does provide a useful operational definition of preflare patterns. These more rapid changes, especially in the corona, were the subject of the third subgroup of the Preflare Activity Team.

1.4.1.1 Review of Previous Studies of Coronal Precursors

Earlier searches for rapid flare precursors involving coronal phenomena recognized the physical importance of the corona for storage and release of flare energy. Reported coronal precursors have included X-ray brightenings associated with filament activations (Rust *et al.*, 1975), expanding and brightening green-line arches (Bruzek and DeMastus, 1970), gradual enhancements and spectral hardening of soft X-ray and microwave flux (Webb, 1983), "forerunners" of white-light transients (Jackson and Hildner, 1978), changes